LAPPEENRANTA UNIVERSITY OF TECHNOLOGY
LUT School of Engineering Science
Degree program in Technical Physics

Kunakovskaya Ekaterina

EFFICIENCY OF UPCONVERSION PROCESS IN LANTHANIDE-DOPED HOST LATTICES

Examiner: Professor, D.Sc. Erkki Lähderanta
Supervisor: Researcher, D.Sc.(Tech.), Regina Gumenyuk

ABSTRACT

Lappeenranta University of Technology
LUT School of Engineering Science
Degree program in Technical Physics

Kunakovskaya Ekaterina

Efficiency of upconversion process in lanthanide-doped host lattices

Master's thesis

2019

72 pages, 35 figures

Examiners: Professor, D.Sc. Erkki Lähderanta
Senior Research Fellow, D.Sc., Regina Gumenyuk

Keywords: upconversion, downconversion, nanoparticles, lanthanide

The main target of this work was to investigate the influence of the host matrix on the upconversion luminescence. The quantum yield was used as a measure of luminescence efficiency. For this, a reliable and sensitive measurement setup was built and calibrated.

The upconversion luminescence efficiency was examined in upconversion nanoparticles, phosphate glasses doped by upconversion nanoparticles and rare-earth dopants, and the rare-earth-doped tellurite glasses.

It was experimentally demonstrated that besides phonon energy of the host material other parameters also play a crucial role in the luminescence efficiency such as surface and water quenching effects, material homogeneity, dopants composition and concentration, and down-conversion as a competitive process.

ACKNOWLEDGEMENTS

This work has been carried out in the Photonics Laboratory at Tampere University. Thus, I would like to express my special thanks of gratitude to my supervisor Dr. Regina Gumenyuk for her kind support and guidance in completing my project. I came to know about so many new things I am really thankful to her.

I would like to thank Professor Erkki Lähderanta for giving me the great opportunity to study in Lappeenranta University of Technology. Finally, I would like to thank my family and friends for their support and encouragement, it helped me a lot.

This work was carried out within the frame of Academy of Finland Postdoctoral Research Project (Project No. 285170).

Tampere, May 2019

Kunakovskaya Ekaterina

LIST OF ABBREVIATIONS AND SYMBOLS

CET – cooperative energy transfer
CW – continuous wave
DC – downconversion
DS – downshifting
EMU – energy migration upconversion
ESA – excited state absorption
ET – energy transfer
ETU – energy transfer upconversion
IR – infrared
LSP – localized surface plasmon
NIR – near-infrared
PA – photon avalanche
PL – photoluminescence
QC – quantum cutting
QY – quantum yield
RE – rare earth
SHG – second harmonic generation
TPA – two photon absorption
UC – upconversion
UCL – upconversion luminescence
UCNPs – upconversion nanoparticles
VIS – visible

CONTENTS

1. INTRODUCTION

The upconversion (UC) phenomenon allows the conversion of low-energy pump radiation from the near infrared region to high-energy luminescence in the visible range. Materials based on this phenomenon are widely distributed, and the scope of their application continues to grow. It can be found from lighting, LEDs, and lasers to volumetric 3D displays and photovoltaic devices. They are also promising for the manufacture of solar cells.

Special attention should be paid to upconversion nanoparticles, which are used in the field of biomedical diagnostics and therapy. The excitations of up-conversion luminescence is driven by laser sources of NIR range referred to the 1st biological window of the tissue. Low water absorption at the pump wavelength ensures the maximum depth of sensing and minimizes the autofluorescence and photodamage of biological tissues [1].

The selection and evaluation of the optimal upconversion phosphors are carried out according to such an important parameter as the luminescence quantum yield, which shows how effectively the exciting light is converted into luminescence in the material. Quantum yield strongly depends on the composition of the material, its purity and "water-free" content. Usually, the phosphors consist of a matrix and dopant ions, embedded into them. To activate the process of up-conversion, rare-earth metals ions are used as the most popular dopants due to its reach energy level systems.

Currently, low value of quantum yield of up-conversion luminescence is one of the main limiting factors for their widespread application. To obtain the maximum efficiency of upconversion luminescence, it is essentially to assort the effective architecture of the phosphor, where one of the most critical roles is devoted to the host matrix. Consequently, the investigation of different matrixes properties and their impact on up-conversion luminescence is indispensable.

The present thesis describes the detailed investigation of upconversion luminescence efficiency in different luminescent materials, involving nanoparticles and glasses doped

with lanthanide ions. The thesis consists of 6 chapters. Chapter 2 provides the necessary basic information of frequency conversion mechanisms. In Chapter 3 upconversion luminescence is considered in more details, including the description of UC materials components, and evaluation of quantum yield efficiency. In Chapters 4 and 5 experimental setup and results of measurement of UC nanoparticles and doped glasses are presented.

2. FREQUENCY CONVERSION

Photon frequency conversion is the conversion of the input light to the light of other frequencies, using optical nonlinearities [2]. Substances that can convert absorbed energy into light radiation that is, luminescence, are called luminophores. Inorganic luminophores are known as phosphors. There are two main processes of photon frequency conversion taken place in the phosphors: upconversion (UC) and down-conversion (DC).

Photon upconversion is a nonlinear optical process of converting long-wave (low energy) exciting radiation into short-wave (high energy) radiation due to the summation of the electronic excitation energy. For the upconversion phosphors, the luminescence wavelength is shorter than the excitation radiation wavelength. It is called the Anti-Stokes shift (Fig.1).

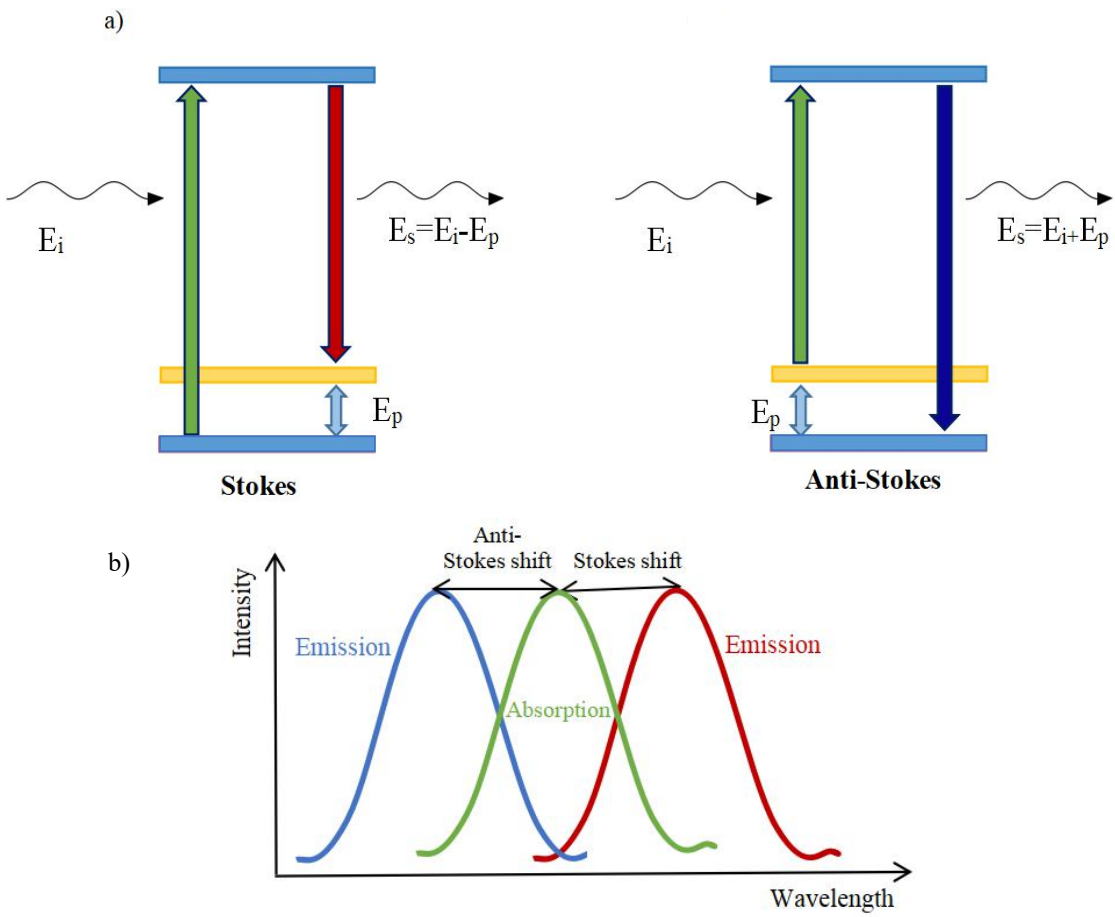

Figure 1. The Stokes and Anti-Stokes shifts. a) Schematic diagrams of energy transfer, where E_i is the energy of the incident photon, E_s is the energy of scattering photon and E_p is the energy of phonon b) Absorption and emission spectra.

The opposite process, *down-conversion*, is the Stokes process, in which a photon with high energy is converted into a photon (or several photons) with low energy (Fig.1a). As a result, the luminescence wavelength is greater than the excitation wavelength (Fig.1b). This process is more common for phosphors than upconversion.

In this chapter, the processes of up- and down-conversions will be considered in more detail, including a description of the mechanisms and comparison with similar luminescence processes.

2.1 Downconversion

DC was first discovered in the early 1970s when it was shown that cascade radiation from the high energy level $^1S_0$ of Pr^{3+} ion can produce two photons in the visible range in a two-step emission process. The cascade emission of Pr^{3+} is found today in a large number of fluoride materials, in which the $^1S_0$ state of the Pr^{3+} ion lies below the 4*f*5*d* states. [3].

To the date, it has been experimentally confirmed that most luminescent materials follow a conventional down-conversion mode: the excitation of higher energy results in the emission of a photon (also known as down-shifting (DS)) or several photons (which is referred to as quantum-cutting (QC)) with lower energy [4]. Schematic representation of these two processes is shown in the Fig.2.

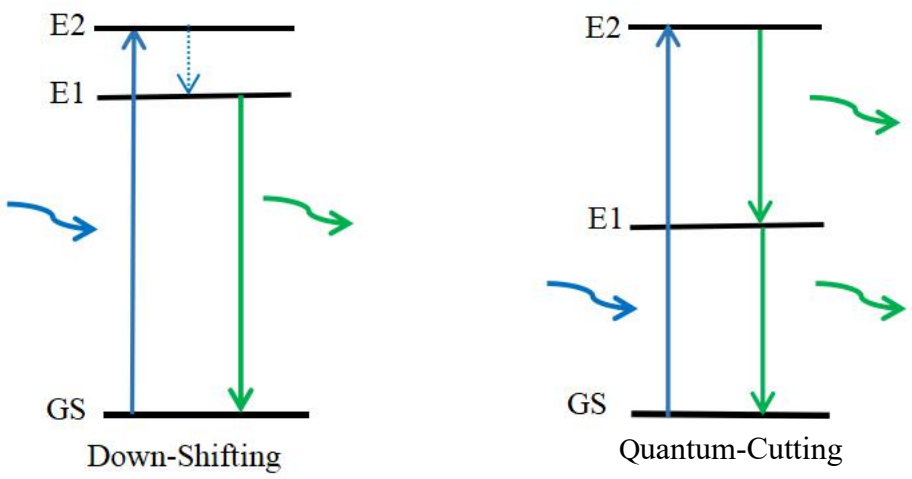

Figure 2. Down-Shifting and Quantum-Cutting processes.

The mechanism of the *down-shifting* can be represented as traditional photoluminescence. Inside the atom, electrons can occupy states with different energies. Moreover, for a substance in order to luminesce, these states must be discrete. As a consequent, the system contains some levels corresponding to a certain value of energy at which electrons can be located. These levels are separated by forbidden energy zones, where the electron cannot reside. The state on which the electron is originally located is called the ground state. If the electron has absorbed external radiation, then the energy of the absorbed radiation is added to its energy, and it passes into the so-called excited state. From an excited state, the electron must return to the ground after some time. For this, it needs to decrease its energy, and it returns the absorbed energy back. However, part of the energy absorbed by the electron is lost due to non-radiative processes, for example, due to the lattice vibration or heat release. As a result, less energy is emitted than absorbed, and the luminescence radiation will have a longer wavelength than the absorbed radiation.

Quantum cutting can be realized in a single ion or several ions system via energy transfer. Figure 3 depicts three possible cases of the QC process. The first case includes one optically active center with three energy levels system. When excited to the energy level E2, the ion emits two photons in order to relax stepwise to the ground state (Figure 3(a)). These photons may have the same or different energies. The second case involves two ions: an excited ion (I) can relax from the state E2 to E1 by transferring energy to the second ion (II) (Figure 3(b)). After energy transfer, both ions can emit a photon to reach the ground state. The condition of energy resonance must be fulfilled, the energy difference for the energy transfer transitions in both ions should be the same. In the third case (Figure 3(c)), QC occurs by using three optically active centers. Ion (I) is excited by a photon. The excited ion (I) can relax into the ground state, E0, by transferring the energy to two nearby ions (II+III). After the energy transfer, both of these centers emits a photon of the same energy [4].

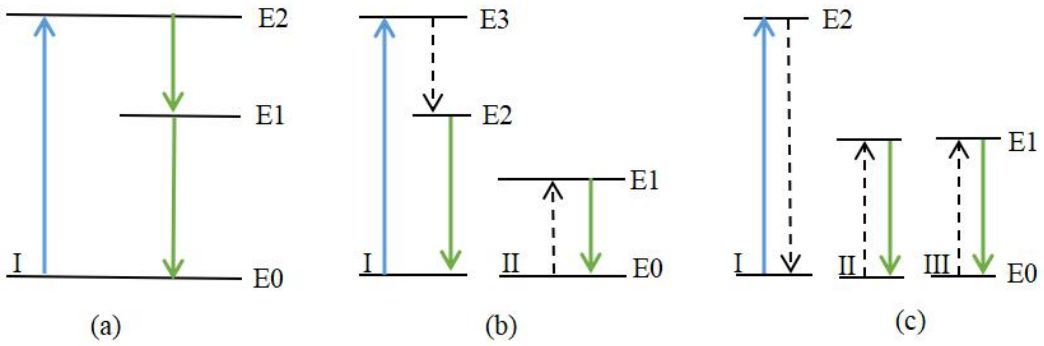

Figure 3. Mechanisms of quantum cutting with one ion (a), two ions (b) and three ions (c).

The principal difference between the DS and QC processes is the number of emitting photons. In the DS one absorbed photon results in the emission of one photon. The difference in the photons' energy is dissipated via the lattice vibrations. In the QC one absorbed photon triggers the emission of two photons, which energy can be the same or different. Both processes are aligned with the energy conservation principle.

2.2 Upconversion

However, more attention is now being paid to the opposite process, upconversion, due to its low excitation energy and opportunity to get visible wavelength emission.

The process of photon upconversion is presented by sequential absorption of two or more photons of low energy and emission of a higher energy photon [5]. This concept was first conceived as a theoretical possibility by physicist Nicolaas Bloembergen in 1959 [6]. The landmark experiment to witness upconverted visible emission was reported in 1966 by François Auzel and was based on energy transfer through the use of Yb^{3+} to Er^{3+} and Tm^{3+}. Such Yb^{3+} upconversion was also observed by Ovsyankin and Feofilov independently in the same year [7].

Upconversion is characterized by low process initiation requirements compared to other Anti-Stokes processes. Therefore, it is highly attractive effect for a potential list of visible light applications. The most well-known physical processes that also lead to the energy increase of the emitted photons relative to the initial energy of photons are a second

harmonic generation (SHG) and two-photon absorption (TPA). Schematically, these processes are shown on Figure 4. Two-photon absorption is a process of transition from the ground state to the real excited state due to the absorption of two quanta, total energy of which is equal to the exiting energy (Fig.4(a)). It is important that two-photon absorption strongly depends on the polarization of the exciting fields, even in the case of an isotropic medium. For the $0 \rightarrow 1$ transition, the simultaneous absorption of two excitation quanta is necessary. For this reason, the observation of Anti-Stokes luminescence as a result of two-photon absorption is possible only at high intensities of excitation. Second harmonic generation is a frequency doubling of the emitted light without absorption at intermediate states (Fig.4(b)). Such process is possible only in a medium without an inversion (symmetry) center. It takes place through a virtual level, and therefore for observation of SHG it is also necessary to use intense exciting radiation. Moreover, to maximize the efficiency of the process, it is necessary to fulfill the phase-matching condition for the fundamental wave and its second harmonic. The intensity of the emitted radiation in the case of the generation of the second harmonic and two-photon absorption depends quadratically on the excitation intensity. In practice, they are realized with the use of pulsed femtosecond lasers, which provide high power densities of exciting radiation, of the order of megawatts per square centimeter. In order to observe the upconversion (Fig.4(c)), intense laser radiation is not required; inexpensive laser diodes, operating in continuous generation mode can be used for excitation. Thus, for observing upconversion in crystals, there are no special requirements to the intensity of the exciting field (it can be ~1-100 W/cm^2), nor to the coherence of radiation. It is important that the excitation process occurs in a cascade manner through the real metastable states, in contrast to the two-photon absorption process, where the virtual level is involved. Consequently, the efficiency of upconversion is higher than the efficiency of two-photon absorption as a process of conversion of exciting radiation, but less than the efficiency of second-harmonic generation (in nonlinear crystals).

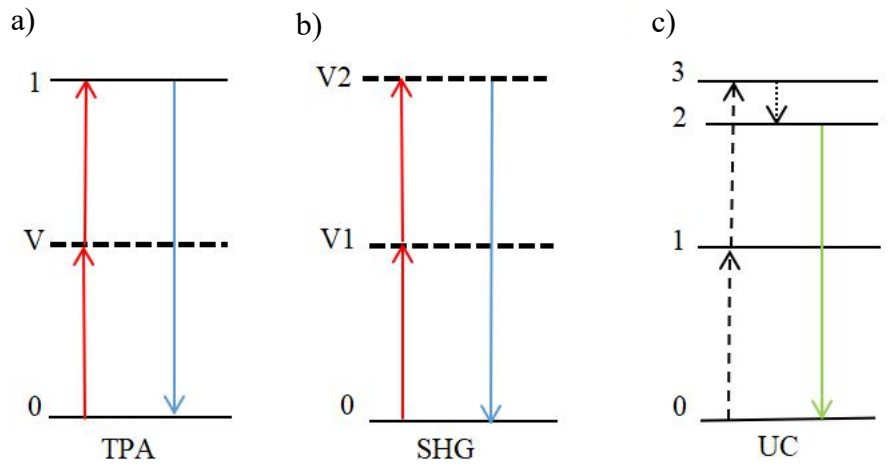

Figure 4. Nonlinear processes leading to Anti-Stokes emission: a) two-photon absorption (TPA), b) second harmonic generation (SHG), c) upconversion (UC).

A typical upconversion process includes several metastable energy states (states with a long lifetime) , such as metastable states 1, 2, and 3 on Fig. 4c. Upon absorption of a low-energy photon, the ground state is populated to metastable state 1, which is then promoted to a higher energy state, metastable state 3, by subsequently absorbing another low-energy photon. Following some internal relaxation processes, metastable state 3 relaxes to a slightly lower excited energy state, metastable state 2, and then jumps to the ground state by releasing photon radiation. [8]

Most of the upconversion materials consist of solid-state matrix, doped with rare-earth ions, chemical elements of the third group, i.e., Sc (21), Y(39), La(57) and 14 elements of the lanthanide family of the Mendeleev periodic system Ce(58), Pr (59), Nd(60), Pm(61), Sm(62), Eu(63), Gd(64), Tb(65), Dy(66), Ho(67), Er(68), Tm(69), Yb(70), Lu(71). For example ZnO:Er, ZnO:Er:Yb thin films, $NaYF_4$:Yb,Er(Tm) nanoparticles, heterostructures consisting of CdSe quantum dots (CdSe/$NaYF_4$:Yb,Er).

2.2.1 Mechanism of upconversion processes

The UC mechanisms can be divided into five classes: (a) excited state absorption (ESA, Fig. 5(a)), (b) energy transfer upconversion (ETU, Fig. 5(b)), (c) photon avalanche (PA, Fig. 5(c)), (d) cooperative energy transfer (CET, Fig. 5(d)), and (e) energy migration

upconversion (EMU, Fig. 5(e)). Each process of energy transfer has its own UC efficiency and that there is no universal mechanism for any of the luminescent Ln^{3+} ions [9].

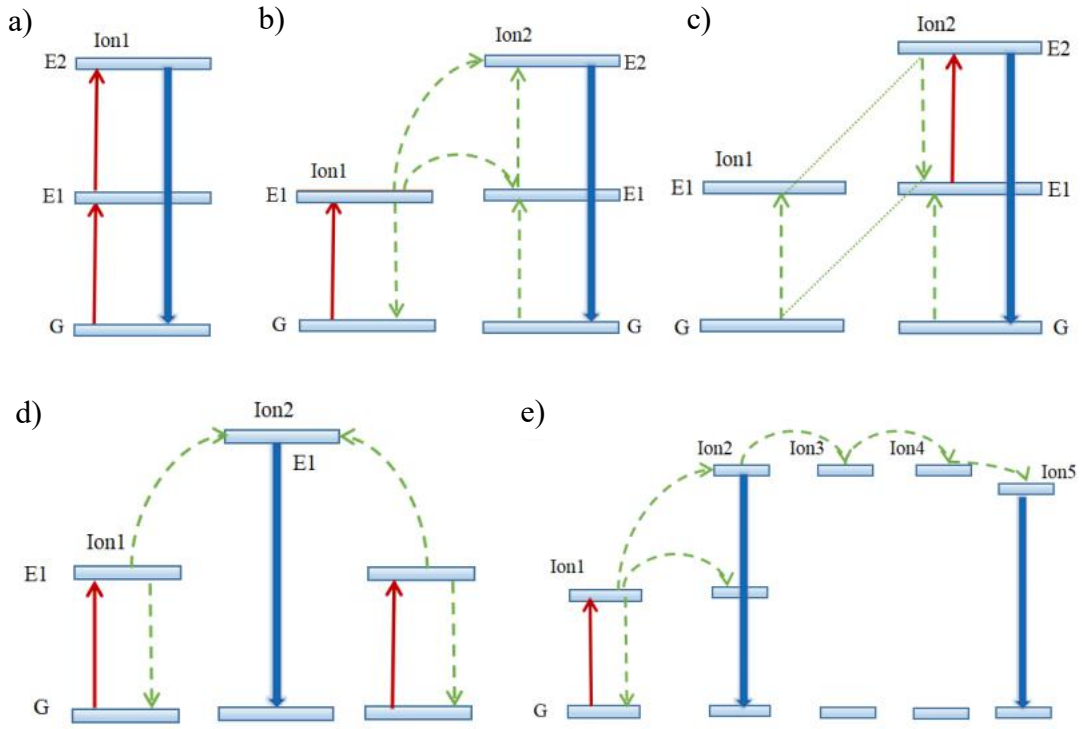

Figure 5. Schemes of upconversion processes: a) ESA, b) ETU, c) PA, d) CET, e) EMU. Red arrow stands for excitation, blue for emission and dashed green represent energy transfer.

In the first process, **ESA**, only one ion participates, sequentially absorbing excitation quanta from the ground state. As a result, the ion is in the second excited state, relaxation from which leads to anti-Stokes luminescence. The efficiency of such a process depends on the absorption cross section of the ion at the excitation wavelength, as well as on the pumping rate and relaxation rate of the first excited state. The states of trivalent rare-earth ions in the crystal matrix often turn out to be long-lived (metastable) due to the low probability of transition, governed by the selection rules. As a result, the excitation of an ion through an intermediate metastable state can be quite effective even at insignificant pump intensities. It is worth noting that for the effective sequential absorption of the exciting radiation it is necessary that the ion energy levels in the matrix should be equidistant. Such "ladder" scheme of levels has ions Er^{3+}, Tm^{3+}, Ho^{3+}, and Nd^{3+}.

The second process, **ETU**, represents the sequential transfer of energy from the first type ion, excited by the radiation source, to the second type ion through a radiative or non-radiative energy transfer channel. In this case, the energies of the first excited states of both ions should be close in value. If the interaction between ions is such that the energy transfer between them is effective, then the second type of ion does not necessarily have to effectively absorb the exciting radiation in order for upconversion to occur. In this regard, the first type of ion is chosen with a large absorption cross-section at the excitation wavelength. Such ion is called a sensitizer. An ion of the second type, acting as an energy acceptor, is called an activator. The efficiency of energy transfer in a sensitizer - activator pair depends on several factors, but primarily on the distance between ions or, in other words, on the concentration of ions.

One of the less studied processes leading to upconversion is a threshold process called the photon avalanche (**PA**). It lets the excitation radiation be non-resonant in energy for the ion (ion2) to the transition from the ground state to the first excited state. It is suggested that there is an ion nearby (ion1), which is also in the ground state. Then, with an increase of intensity of the excitation, at some moment the second ion will be excited to the first state, and then resonantly excited by radiation to the second level above. The excitation to the first level can occur both under the influence of exciting non-resonant radiation, and because of any other process. Next, a cross-relaxation occurs between the first and second ions: E2 (ion2) + G (ion1) → E1 (ion2) + E1 (ion1). As a result, both ions are in the first excited state. The second ion again absorbs intense exciting radiation and passes into a state from which relaxation with anti-Stokes luminescence can occur. The avalanche nature of the process is that cross-relaxation with neighboring ions acts as a feedback, and as a result of each “cycle” of the process, a pair of ions is formed in the first excited state, from which resonant absorption is efficient. The effectiveness of the described process is determined by the concentration of ions and demonstrates a threshold dependence on the intensity of the exciting radiation. PA-related UC emissions are much less efficient, especially in nanomaterials.

The next process is called cooperative energy transfer (**CET**). The activator ion, which is initially in the ground state, is excited by the energy of two ion-sensitizers, each of which

absorbs IR quanta of exciting radiation. In this case, the sensitizing ions can be both the same and different rare-earth ions. It is important to note that the efficiency of cooperative sensitization is several orders lower than the efficiency of the ESA and ETU since the excitation occurs through the virtual level, and not through a real metastable state.

One-step energy transfer between the donor and the acceptor ends at the acceptor's energy system. However, with a high concentration of donors, is possible the migration of excitation energy (**EMU**) in the donor ensemble, which occurs before the transfer of electronic excitation energy to the acceptor. The effect of migration on luminescence parameters must be taken into account since it "expands" the effect of other types of excitation transmission. So migration by donors can bring excitement to a remote acceptor, which will increase the efficiency of luminescence sensitization. At the same time, non-radiative degradation of the energy of metastable donor states can occur, which reduces quantum yield and average luminescence duration. The phenomenon of concentration quenching is explained by an increase in the migration of excitation with the "delivery" of excitation to the centers located near luminescence quenchers. It greatly increases the probability of non-radiative processes [10-12].

3. UPCONVERSION LUMINESENCE

Most of the conventional materials have luminescent radiation with a Stokes shift, which is a down-conversion process and describes the conversion of a high-energy photon into a photon with lower energy. Usually, such a process is also called photoluminescence (PL). By absorbing a photon, the optically active center passes into an excited state. By emitting a photon with the same or lower energy in comparison with the exciting one, the active center returns to the ground state [13].

In contrast, upconversion luminescence is an anti-Stokes process. Non-coherent and low-power sources, such as standard xenon or halogen lamps, continuous wave lasers (CW), or even focused sunlight can be used as a source of excitation for this process. The general principle of the upconversion luminescence processes shown on Fig.6, which demonstrates the difference from the traditional PL process. A luminescent center in ground state 1 can absorb energy from the corresponding energy transfer process (ET) or from the excitation photon to reach the excited state 2. Then another excitation photon or a corresponding ET process will transfer the luminescent center to the excited state 3. A radiative transition from the excited state 3 back to the ground state or to another state with lower energy, results in the emission of photons with higher energy. For the upconversion luminescence process, a metastable intermediate excited state is actually achieved. This is different from the TPA process. It is expected that this metastable level will have a relatively long lifetime in order to maintain a high population in the intermediate excited state before the second excitation energy. [14]

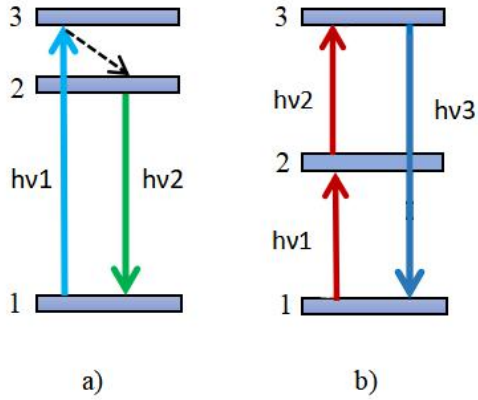

Figure 6. Schematic representation of (a) Conventional Photoluminescence and (b) the Upconversion Luminescence processes.

The up-conversion luminescence arises due to 4f - 4f orbital electronic transitions with accompanying wave functions localized inside a single lanthanide ion. These internal 4f electronic transitions of lanthanide ions are electrical dipoles, forbidden by the rules of quantum mechanical selection, which, however, are weakened due to local crystal field-induced mixing of the f-states with higher electronic configurations. Due to the forbidden nature of the 4f - 4f transition, the energy levels of lanthanide ions have very large (up to 10s of milliseconds) lifetimes, which contributes to successive excitations in the excited states of one lanthanide ion and also allows energy transfer between two or more lanthanide ions. These resulting properties of lanthanide dopants determine the main mechanisms upconversion luminescence process.

The upconversion luminescence intensity generally has a nonlinear dependence on the excitation light density:

$$I\text{uc} = KP^n \qquad (1)$$

Where I_{UC} is the luminescence intensity, K is material related coefficient, P is the power of pump laser, and n is the number of the excitation photons required to produce the upconversion luminescence [8].

3.1 Lanthanide ions upconvertors

Lanthanides are 15 elements (elements of III group of the 6th period of the periodic table. They are metals with atomic numbers 57-71 (from lanthanum to lutetium)) in which 14 4f-electrons are sequentially added to the electronic configuration of lanthanum.

In the lanthanide atom, a deep-lying fourth layer of 4*f*14 is filled. Thus, only 14 lanthanides can exist. Since the structure of the two outer electron shells does not change as the core charge increases, all lanthanides have similar chemical properties.

The unique properties of lanthanides, which lie in their ability to luminesce in a wide range of wavelengths (Fig.7), including the ultraviolet, VIS and NIR regions, make them possible applicants for various applications, such as laser and fiber optic technology, photodynamic therapy and diagnostics.

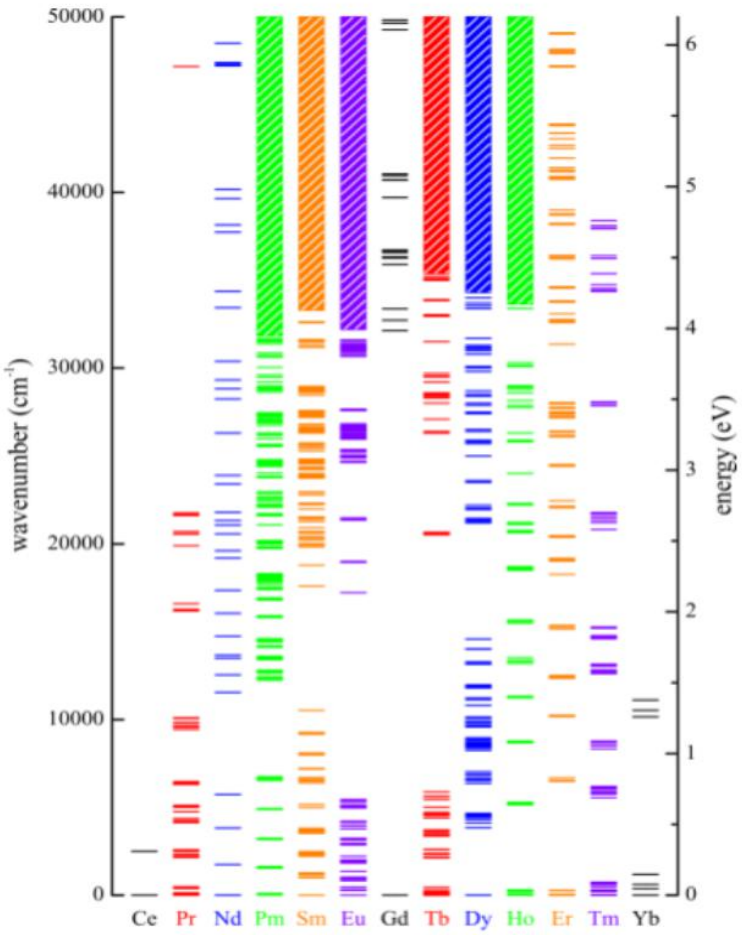

Figure 7. Energy levels of the 4fn configurations of the trivalent rare earth ions. Closely spaced levels are depicted as bands [3].

Rare-earth elements usually pass into the ionized trivalent state, giving up two electrons from $6s^2$ orbital and one electron from 5d or 4f orbitals. The electrons in the 4f shell are shielded by the outer $5s^2$ and $5p^6$ shells. As a result, the position of the energy levels of lanthanides, which are characterized by spin-orbit interaction, very little depends on the environment and remains almost the same for the same ion in different matrices. In this case, the energy state of the sublevels is completely determined by the nearest environment of the rare-earth ion, due to the Stark effect (shift and splitting into sublevels of energy levels of atoms and other quantum systems under the influence of electric fields). In general case, lanthanide ions can pass into the excited state through three types of transitions: 4f-4f and 4f-5d, as well as charge-transfer transitions (Fig. 8). Upconversion luminescence occurs as a result of 4f -4f transitions.

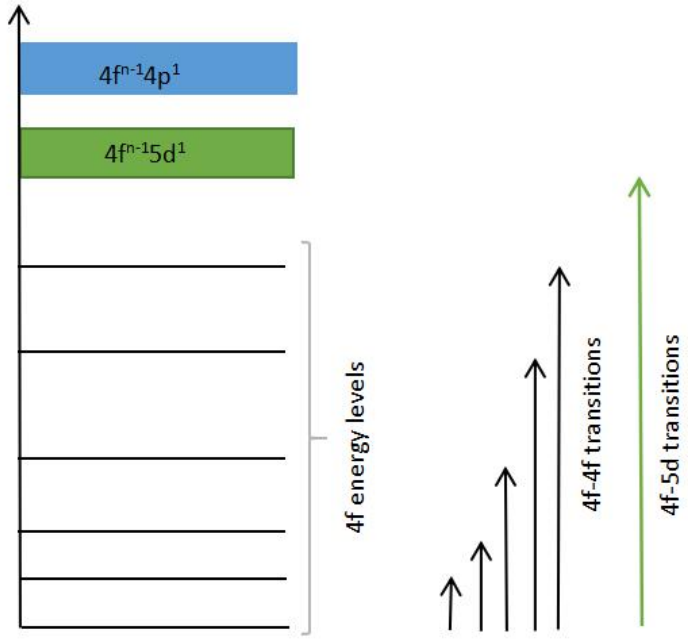

Figure 8. Schematic of the excitation of lanthanide ions 4f-4f and 4f-5d transitions.

These transitions occur during passages between different energy levels of the 4f orbitals inside one ion. Electron-dipole 4f-4f transitions are prohibited by the Laporte rule. In crystals with symmetry of the nearest environment below the cubic, prohibition can be partially lifted. In this case, narrow luminescence bands are observed, whose position depends on the specific symmetry of the nearest environment of the rare-earth ion. The effective spontaneous emission and absorption cross sections associated with 4f – 4f transitions are small, which affects the long luminescence lifetime compared with other phosphors.

To describe the process of upconversion luminescence in detail, let's consider a pair of ions Yb^{3+} and Er^{3+}. Doping with these ions makes it possible to obtain luminescence from the UV to the IR spectral range, including the luminescence band in the visible range with the upconversion excitation mechanism in the NIR range. The scheme of realization of upconversion in the Yb^{3+} - Er^{3+} ion system is presented in Fig.9.

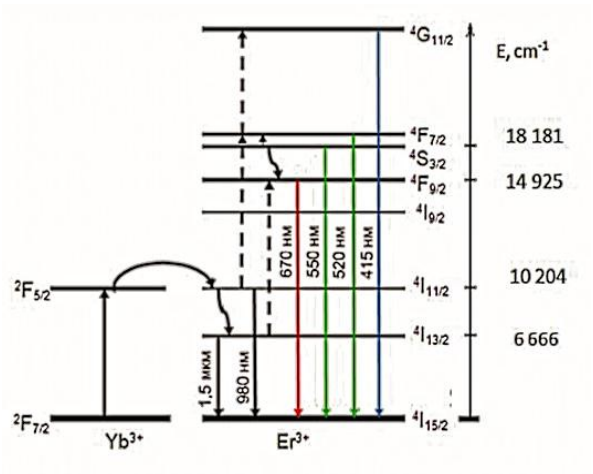

Figure 9. The scheme of upconversion realization in the system of ions Yb^{3+}-Er^{3+} [15].

The Yb^{3+} ions, which is donor ions, have high effective absorption cross-section in the IR region. The energy states of the acceptor ion, Er^{3+}, have a long lifetime; therefore, the donor ion can transfer to the long-lived acceptor state several absorbed photons simultaneously, resulting in an increase in the energy of the excited metastable state and, accordingly, a decrease in the luminescence wavelength. When irradiated, the Yb^{3+} ion (donor) absorbs a photon, as a result of which a transition to the excited state of $^2F_{5/2}$ occurs. Then it relaxes to the ground state of $^2F_{7/2}$, non-radiatively transferring energy to the nearest ion of the acceptor, which then passes into the $^4I_{11/2}$ state. In addition to energy transfer, the Er^{3+} acceptor ion can absorb a quantum of exciting radiation directly and also go to the $^4I_{11/2}$ state, but the probability of such a process is much lower.

Further process can have two ways of development. If the next act of energy transfer or absorption of the acceptor ion from the excited state happens in a shorter time, than the lifetime of the Er^{3+} $^4I_{11/2}$ state, the acceptor will pass to the $^4F_{7/2}$ state, from which it non-radiatively relaxes to the $^4S_{3/2}$ state, and then goes to ground state, emitting a quantum of light in the green part of the spectrum. If the lifetime of the $^4I_{11/2}$ metastable level turns out to be less than the time after which the second energy transfer occurs, then the Er^{3+} ion will have time to switch to the more long-lived $^4I_{13/2}$ state. Then the subsequent transfer of energy from the donor will transfer the acceptor to the $^2F_{9/2}$ state, from which it relaxes to the ground state with radiation in the red region of the spectrum [16].

3.2 Components of Upconversion Luminescence materials

Most of the upconversion materials is a guest-host system, which are based on the guest-RE ions, doped into the host solid crystal or glass matrices. One of the ions serves as a sensitizer or donor (most often Yb^{3+}), and the other serves as an activator or acceptor (Er^{3+}, Tm^{3+}, Ho^{3+}). Activator emits the radiations, and sensitizer acts like a donator of the energy (Fig.10).

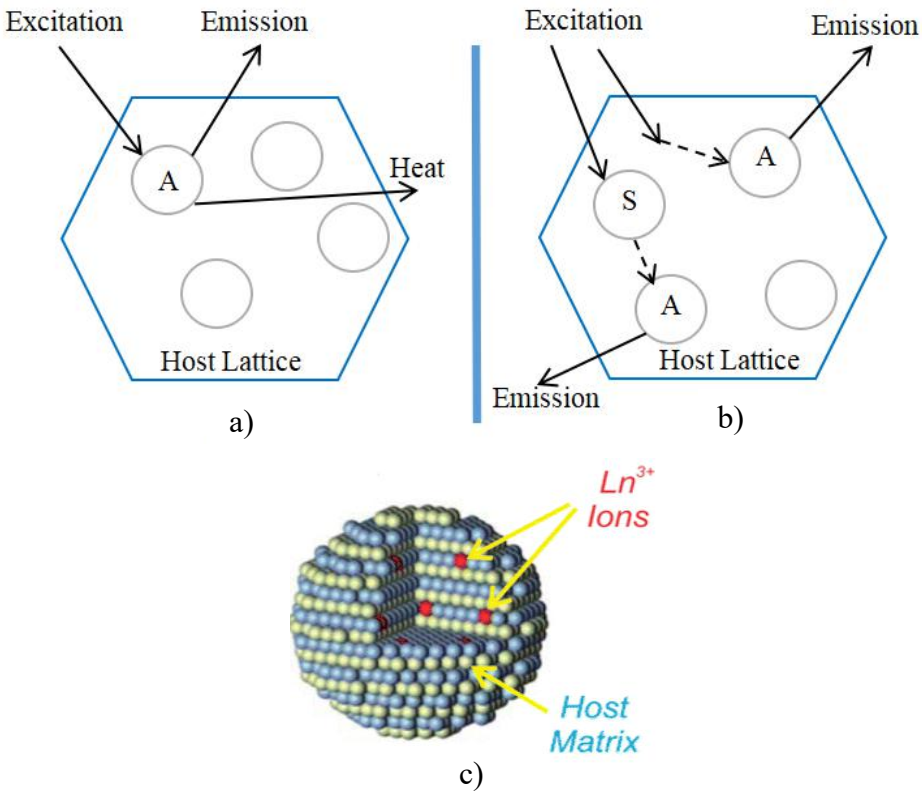

Figure 10. Scheme showing a) direct excitation of the activator (A) and b) indirect excitation followed by energy transfer from the sensitizer (S) or host to the activator (A). Dashed arrow indicates energy transfer [17]. c) Schematic representation of lanthanide dopant ions embedded in the nanocrystal host [18].

3.2.1. Sensitizer

The sensitizer is called an ion, which absorbs the exciting radiation and transmits energy to the activator (Fig.11).

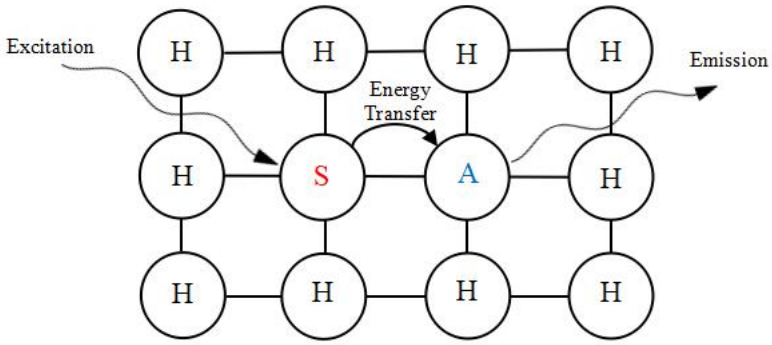

Figure 11. Luminescent material with energy transfer from a sensitizer to an activator.

The sensitizer is able to effectively absorb the IR photon and move from the ground to the excited metastable state. The excited ion-sensitizer in the simplest case transfers energy to the activator-ion due to the radiative and non-radiative channels of quasi-resonant energy transfer. The efficiency of non-radiative transfer of energy between the sensitizer and the activator ions is determined by the matrix, the concentration of ions in the matrix, the overlap of the emission spectra of the sensitizer and absorption of the activator. Multiple energy transfer from the excited sensitizer to the activator and the absorption of exciting IR radiation by the sensitizers ions leads to the fact that the activator ions are in states with greater energy than the energy of the exciting IR quantum. Relaxation of such states leads to anti-Stokes luminescence.

Most often, the Yb^{3+} ion is used as a sensitizer for Er^{3+} and Tm^{3+} due to its large absorption cross-section at a wavelength of 980 nm, which is 1.2×10-20 cm^2, an order of magnitude higher than the absorption of erbium in this region (1.7×10-21 cm^2) [19]. The ion concentrations of the sensitizers typically 20-40 mol.%. However, when the concentration of the sensitizer is much higher than optimal, there is a strong decrease in intensity due to the reverse transfer of energy to ytterbium ions. Also, sometimes, neodymium ion is used as a sensitizer.

3.2.2. Activators

Activator ions act as the centers of luminescence, while sensitizing ions increase the intensity of upconversion luminescence. Among the up-conversion materials, the most

commonly used activator ions are Er^{3+}, Tm^{3+}, and Ho^{3+}, which have a branched structure of energy levels and abundant electronic states.

The choice of the activator ion determines the spectrum of up-conversion luminescence. During the process of energy transfer, activator's electrons at the ground state level absorb energy from nearby excited sensitizers to carry out further transition and become excited to the intermediate level. If the energy levels of the activators are close to each other the up-conversion leads to undesirable non-radiative relaxations. The UC emissions of activators in their typical hosts are presented in Table 1.

Activators	Hosts	UC emissions (nm)
Pr^{3+}	KPb_2CI_5, $Gd_3Ga_5O_{12}$	485, 520, 538, 605, 635,645, 670, 690, 720
Nd^{3+}	YVO_4, Pb:TeO_2	430, 482, 525, 535, 580, 600, 664, 766
Sm^{3+}	$NaYbF_4$, $NaGdF_4$	520, 541, 555, 590, 646, 657, 700, 799, 873
Eu^{3+}	$NaGdF_4$, Gd3Ga_5O_{12}, $Y_3AI_5O_{12}$	416, 429,490, 510, 535, 554, 590, 613
Gd^{3+}	$NaYF_4$	278,305,312
Tb^{3+}	$NaGdF_4$, α-$NaYF_4$, $Gd_3Ga_5O_{12}$, $Y_3AI_5O_{12}$	381, 415,438, 489, 541, 584, 619
Dy^{3+}	AI_2O_3, $NaGdF_4$	378, 408,487, 543, 569, 570, 610, 655, 663
Ho^{3+}	LaF_3, Y_2O_3	542, 655
Er^{3+}	$NaYF_4$	415,525,542, 655
Tm^{3+}	$NaYF_4$	290, 345, 362, 450,475,644, 694, 800
Yb^{3+}	$YbPO_4$	450-500

Table 1. Typical activator-host combinations and corresponding UC emissions [20].

3.2.3 Host Matrix

In addition to dopant ions, the structure of the host lattice and its interaction with the sensitizer and activator ions has a strong influence on the upconversion process. The material of host lattice determines the distance between the dopant ions, their relative

spatial position, coordination numbers, and the type of surrounding anions. There are two most important requirements for host lattice materials, low lattice mismatch to the doping ions and low phonon energy [8].

Phonon energy is the resonant energy caused by lattice vibrations. In the rare-earth metals, it is important to take into account these fluctuations due to the fact that a large number of phonons are involved in the relaxation process.

Since the energy of the phonon greatly affects the efficiency of the upconversion process, in the ideal host materials it must be low. The phonon energy values for some matrix materials are presented in Table.2.

Material	**Phonon energy (cm^{-1})**
Phosphate glass	1,200
Silica glass	1,100
Tellurite glasses	750
Fluoride glass	550
Chalcogenide glass	400
Y_20_3	550
$Zr0_2$	500
$NaYF_4$	350
LaF_3	300
$LaCl_3$	240
YVO_4	890
Y_2O_2S	520
GdOCl	500
$LaP0_4$	1,050
$MgCl_2$	100
$CsCdCl_3$	620
Cs_2NaYCl_6	600
Cs_2ZrCl_6	2,300
Cs_2ZrBr_6	2,600

Table 2. Phonon energy of the most frequently used matrices for rare-earth ions [8].

It is important to select properly the composition of the host matrix in order to maximize radiation and minimize non-radiative losses. Usually, heavy halides, such as iodides,

chlorides, and bromides, have low phonon energy (under 300 cm^{-1}). However, due to their hygroscopicity, they are not widely used. Oxides are much more chemically stable, but their phonon energies are higher, more than 500 cm^{-1}, due to the stretching vibration of the host lattice. For comparison, usually high chemical stability and low phonon energy have fluorides (350 cm^{-1}) and therefore are often used as the host materials. In addition to the aforementioned materials, semiconductor nanocrystals such as ZnS have also been proposed as a possible alternative. However, it is still a contentious issue, whether lanthanide ions are included in these nanocrystals homogeneously in the host lattice or located on the outermost layer of the nanocrystals due to the substantially different size of the ions between the dopant and the host ions [8].

Ideal host materials for upconverting phosphors are inorganic compounds based on trivalent lanthanide ions since all of them have the same chemical properties and size. Also, host lattices based on cations such as Na^{+}, Ca^{2+}, Sr^{2+} and Ba^{2+} with ionic radii close to radii of the lanthanide dopant ions, prevent lattice stresses and defects in crystal and thus are good options for the host materials. Therefore, fluorides based on Na^{+-}, Ca^{2+-} and Y^{3+-} are the best upconversion host materials. For example, the up-conversion efficiency of $NaYF_4$:Yb^{3+},Er^{3+} is 20 times higher than that of La_2O_3:Yb^{3+},Er^{3+} and six times higher than that of $La_2(MoO_4)_3$: Yb^{3+},Er^{3+} [21].

Also, the optical properties of upconversion materials strongly depend on the choice of the crystal structure. The most effective host material for blue and green phosphors with upconversion among the fluoride hosts is a hexagonal $NaYF_4$ (β-$NaYF_4$). The efficiency of the upconversion of hexagonal phase $NaYF_4$:Yb/Er bulk materials is about 10 times higher than in cubic phase analogues. The phase-dependent optical property can be directly attributed to various crystal fields around trivalent lanthanide ions in matrices of different symmetry. Hosts with low symmetry usually have a crystal field containing more uneven components around the dopant ions compared to analogues with high symmetry. The uneven components enhance the electron coupling between the 4f energy levels and the higher electron configuration and subsequently increase the probabilities of the f – f transition of the dopant ions. Moreover, the efficiency of upconversion can also be increased by reducing the size of the cation (or unit-cell volume) of the host, which leads to the increase in the strength of the crystal field around the doping ions. For instance, the

bulk material of $NaYF_4$:Yb/Er exhibits luminescence with an increase in frequency, two times stronger than that of $NaLaF_4$:Yb/Er [8].

Currently, powder or single-crystal matrices are most often used as luminescent matrices. However, the glass may well compete with these materials, winning in the majority of powder phosphors in transparency and resolution, and in crystalline ones - in cost and possibility of manufacturing of various shapes and sizes. In addition, in the case of using fiber glass, it is possible to obtain an effective radiation conversion even at low concentrations of the introduced activator (~ 10^{18} cm^{-3}) due to weak concentration quenching and a significant amount of optical path.

3.3 Quantum yield efficiency

In order to objectively evaluate the brightness of the luminescence, it is necessary to quantify the ability of upconversion materials to absorb and convert the exciting radiation into the required wavelength range. Such quantitative characteristic is called quantum yield (QY). It is numerically equal to the ratio of the number of photons emitted in the visible part of the spectrum, to the number of photons absorbed in the NIR region:

$$\mathrm{QY} = \frac{Nemitt.}{Nabs.} \qquad (2)$$

For upconversion materials, the efficiency of upconversion is often used as a measure, which is numerically equal to the ratio of the power emitted in the visible range to the power absorbed in the NIR range:

$$\mathrm{UCQE} = \frac{Pemiss.(\lambda)}{Pabs.(\lambda)} \qquad (3)$$

The low UC quantum yield is, perhaps, the main disadvantage of upconverting phosphors. Theoretically, the efficiency of the upconversion process is determined by the probability of absorption, relaxation, transfer of electronic excitation and electron-phonon interaction. These parameters are affected by distance between ions, symmetry of the immediate environment, presence of quenching impurities and the transfer of energy to the impurity

ions, energy migration by donor ions and the pump power density [22]. Most approaches for improving efficiency are based on reducing the number of quenching centers and increasing the probability of absorption. The choice of the matrix material, concentration of doping impurities, as well as the methods of synthesis (influence on size, shape, crystal structure, surface properties) are important for obtaining efficient upconversion phosphors. Upconversion process efficiency is low due to nonlinear nature for a two-photon UC process. With energy conversion of two excitation quanta into one emitted photon the quantum yield is limited to 50% and for a three-photon process 33%. A similar principle can be observed in the case of down-conversion when high energy photon results in the emission of two photons with lower energy, and thus a quantum yield higher than 100% can be achieved. Process of down-shifting is similar to the DC, but in that case, only one photon is emitted and some energy is lost due to non-radiative relaxation. That's why quantum yield of DS is lower than 100%.

3.4 Upconversion Luminescence in Ln-doped glasses/fibers

Optical glasses doped with RE ions, due to their ability to convert IR radiation into the visible light, are widely used in various fields, like medical diagnostics, data recording, and storage systems, optical sensors, 3D displays. Compared with bulk optical devices, active fibers have such advantages as good environmental stability, high laser beam quality, low optical losses, flexibility, compact sizes, and good thermal properties. The efficiency of the upconversion process depends strongly on the type of the used host-matrix, and especially on the phonon energy. The lower of the maximum lattice vibrations frequency $h\omega_{max}$ leads to a higher probability of energy conversion. The most common silica glass is a well-known glass with high bandgap- and high phonon-energy. Silica fibers are characterized by low losses in the VIS spectrum, but they are not quite good candidates for upconversion optical fibers due to the relatively short lifetime of excited levels related to upconversion emission, and high probability of multiphonon processes.

Low-phonon energy materials (300-600 cm^{-1}) include fluoride and heavy metal oxide glasses (HMO), however, low mechanical and thermal resistance makes it difficult to use these types of glasses in the manufacture of optical fibers. Higher thermal stability and

relatively low phonon energy (750 cm^{-1}) have tellurite glasses, which makes them suitable for use in the production of upconversion materials [23].

Another advantage of tellurite glasses among possible glassy materials to host RE ions is their ability to ignite upconversion mechanisms. It is possible because they possess such properties as high refractive index, ability to accept large ion concentrations without clustering and, what is of more importantance for the upconversion mechanism, low phonon energy. Similar to fluoride glasses, the low phonon energy of tellurite glasses provides a long lifetime of metastable states, through which electrons transfer to the upper levels, and this leads to visible radiation. For example, the typical lifetime of the $^4I_{11/2}$ Er^{3+} level in tellurite glass is 200 µs, while in quartz glass its value is less than 10 µs. In addition, using trivalent ytterbium Yb^{3+} as a sensitizer increases the efficiency of upconversion. Due to the simple energy structure and high absorption cross-section, the Yb^{3+} ion provides an efficient way of energy transfer to the acceptor ion with limited backward energy transfer from the latter. Moreover, the presence of Yb^{3+} ions makes it possible to use bright commercial IR single-mode laser diodes of 980 nm for pumping [24].

3.5 Upconversion Luminescence in Ln-doped nanoparticles

Upconversion nanoparticles (UCNPs) are dilute guest–host nanosystems with a dimension of less than 100 nm, in which trivalent lanthanide ions, possessing a ladder-like hierarchy of long-lived electronic energy levels, are incorporated in an appropriate dielectric host lattice [25].

The UCNPs are able to emit ultraviolet, visible or near infrared upconversion luminescence (UCL) when excited, typically in the NIR range, through sequentially absorbed two or more low-energy quanta via inter-mediate long-live electronic states to populate higher-lying electronic states. The UCNPs have distinct advantages over other luminescent materials employed in biological applications (i.e., organic dyes, fluorescent proteins, and quantum dots), such as spectrally distinct and narrow emission, non-blinking, and unique photostability. Owing to the large anti-Stokes shift of UCL, the use of UCNPs in bioimaging eliminates the auto- fluorescence background, creating high contrast images.

Due to their exceptional optical properties, UCNPs have attracted broad interest in research areas such as bio-sensing, nano-thermometry, drug delivery, and photodynamic therapy; they are also employed for solar cells and displays [25]. Thus, UCNPs have been considered promising alternatives for traditional phosphors. However, compared to conventional phosphors, the quantum yield of lanthanide-doped UCNPs are relatively low (less than 1%) and about an order of magnitude lower for the corresponding upconverting bulk materials [26].

The optically active centers that produce emission upon excitation in UCNPs are lanthanide dopants. By appropriately selection of lanthanide dopants for UCNPs, wavelength- (color) selective UC can be achieved, such as visible (blue, green and red), NIR to shorter NIR, or ultraviolet radiation. The optical properties of upconversion nanoparticles are similar to those of the corresponding bulk forms. Due to the well-shielded 4f-4f orbital electron transitions by the outer complete 5s and 5p shells, they both produce the same peaks of upconversion luminescence. However, because of surface effects caused by nanoscale, the relative intensity between different luminescence peaks and the efficiency of upconversion nanoparticles are quite different from their bulk counterpart. Due to the high surface-to-volume ratio of the nanoparticles, most of the lanthanide dopants undergo a surface deactivation (because of surface defects, as well as to ligands and solvents that have high phonon energy). Surface-related deactivations incorporate two options: (1) dopants located on or around the nanocrystal surface can be deactivated directly by adjacent surface quenching centers and (2) the energy contained in dopants located in the center of the upconversion nanoparticles can randomly migrate and travel a long distance to the dopant on or around surface or directly to the surface quenching sites [8].

To reduce the effects of surface quenching mentioned above, and therefore, to significantly increase the luminescence intensity, the design of core-shell structures was proposed (Fig. 12). Growing a shell on the surface of nanoparticles allows increasing the distance between lanthanide ions and surface ligands of high vibrational states and, at the same time, reducing the non-radiative energy transfer of the dopants from the core to the surface of nanoparticles.

The host material of the most shells that reduce the quenching effects on the surface of UCNPs is identical to the material of the core, but without dopants. However, other crystalline materials can also be used if (i) the shell material is chemically stable, (ii) the crystal lattice has a low phonon energy, in order to avoid non-radiative processes, and (iii) the core and the shell lattices have similar crystal structures to decrease non-radiative processes caused by crystal defects [27].

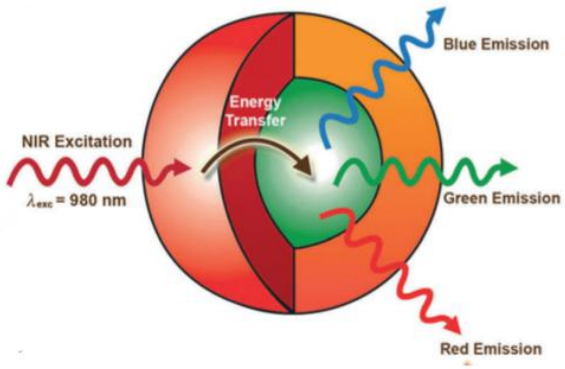

Figure 12. General depiction of the core−shell UCNPs architecture [28].

4. MEASUREMENT OF QUANTUM YIELD

Quantum yield is a measure to quantify the efficiency of energy transfer between exiting and emitting lights via the guest-host system of luminescent phosphors. There are two common approaches for measuring the quantum yield: *relative*, in which the sample under study is compared with the known standard, and *absolute*, using the definition of quantum yield as the ratio of the number of emitted and absorbed photons.

For a relative measurement of the quantum yield, the QY of the sample under study is determined by the formula:

$$QY_{rel.} = QY_s * \frac{E_x}{E_s} * \frac{A_s(\lambda_s)}{A_x(\lambda_x)} * \frac{I_s(\lambda_s)}{I_x(\lambda_x)} * \frac{n_x^{\ 2}}{n_s^{\ 2}} \qquad (4)$$

Where QY_s is the quantum yield of the reference sample, E_x and E_s area under the luminescence spectrum of the studied sample ("*x*") and the reference sample ("*s*"), respectively, $A_s(\lambda_s)$ and $A_x(\lambda_x)$ are the absorption at the excitation wavelength for both samples, $I_s(\lambda_s)$ and $I_x(\lambda_x)$ are the intensity of the exciting beam at the excitation wavelength for both samples, and n_x, n_s is the refractive indexes of the samples. The $I_s(\lambda_s)/I_x(\lambda_x)$ factor can usually be eliminated by measuring the reference sample and the test sample under the same conditions at the same excitation wavelength. In addition, if the excitation wavelength is the wavelength at which the absorption spectra of the reference sample and the sample under study intersect, the factor $A_s(\lambda_s)/A_x(\lambda_x)$ becomes equal to 1, and the expression is simplified to:

$$QY_{rel.} = QY_s * \frac{E_x}{E_s} * \frac{n_x^2}{n_s^2} \qquad (5)$$

The method of relative quantum yield is the most frequently used because of its simplicity, low cost and high sensitivity, which allows measuring small amounts of the sample, and also provides measurements of small quantum yields. For the simplest cases of transparent dilute solutions of small organic dyes, this procedure is considered as the standard, but difficulties arise with wider use. Most often, errors occur when correcting the measured emission spectra for a specific spectral sensitivity of the instruments and the reliability of the reference QY value, which is usually taken from the literature. The QY values of many even recommended quantum yield reference/standards, are still discussed, because these

compounds are often not well characterized for all parameters affecting QY, such as excitation wavelength, temperature, and dye purity. The certified quantum yield standards that can solve these problems are not currently available. In addition, this method is usually based on the samples characterized by identical excitation wavelengths and absorbed light within the matching limits. The same wavelength regions are also used for the emission spectra in order to reduce the systematic deviations associated with the spectral correction of the emission spectra of the sample and the reference.

Despite on the advantages (high sensitivity and simplicity) of the relative measurement technique, it is not applicable for the samples that absorb and emit beyond 600 nm wavelength, since the serious luck of the reliable standards for quantum yield in the near-infrared spectral region [29]. However, these samples are increasingly used in the clinical diagnostics and molecular imaging nowadays, therefore, it is important to certify them qualitatively. For the samples, which absorb and emit in the NIR wavelength range the second technique of absolute QY measurement is applied.

For the evaluation of the absolute quantum yield, the procedure requires to measure under the same conditions the following spectra: the luminescence spectrum of the sample under study (Ec), the luminescence spectrum of the empty cell (Ea), the spectrum of the sample scattering (Lc), and the spectrum of the empty cell scattering (La) . Since the luminescence intensity of the sample corresponds to (Ec-Ea), and the absorption - (La-Lc), the quantum yield can be expressed as:

$$QY_{abs.} = \frac{E_c - E_a}{L_a - L_c} \qquad 6)$$

A spectrum example for determining QY is shown in the figure 13.

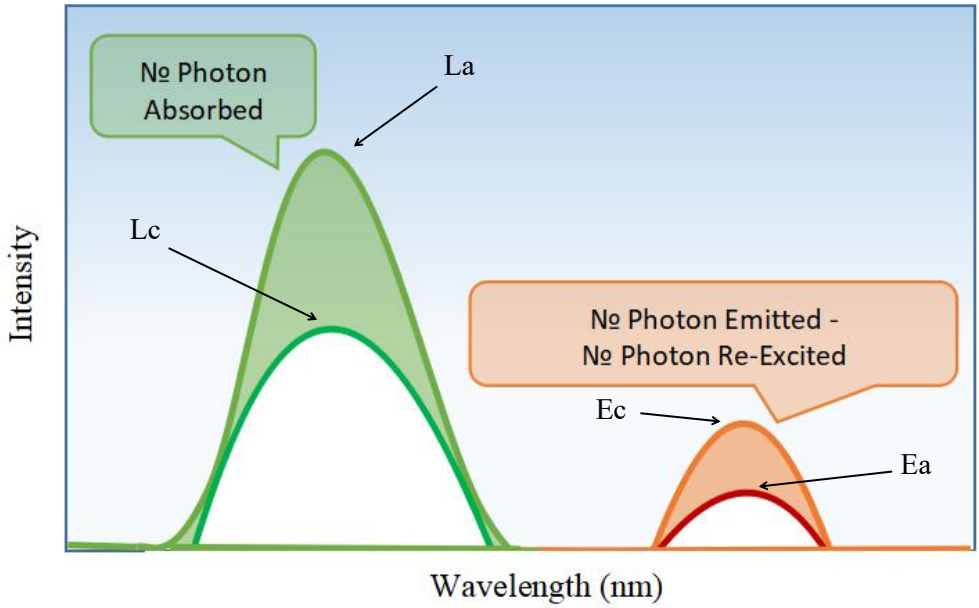

Figure 13. Determination of the quantum yield spectrum.

Taking into account that QY is defined by the ratio between emitted and absorbed photons, the final formula for absolute quantum yield calculation will be:

$$QY = \frac{\int k(\lambda) * (E_c(\lambda) - E_a(\lambda)) d\lambda}{\int k(\lambda) * (L_a(\lambda) - L_c(\lambda)) d\lambda} \qquad 7)$$

Where Ec is the luminescence spectrum of the test sample at the corresponding wavelength, Ea the luminescence spectrum of the empty cell, Lc the spectrum of the sample scattering, La the spectrum of the empty cell scattering and k is a calculated calibration coefficient, related to the used equipment.

The absolute quantum yield method avoids the uncertainties related to the use of fluorescence standards observed in the relative measurement method. In addition, it is the only fluorometric method suitable for measuring QY values of scattering systems. The main factors determining the accuracy of absolute measurements of QY are the correct consideration of the effects of re-absorption and the reliability of the radiometric characteristics of the integration sphere setup. Inaccurate estimation of these factors can lead to significant systematic errors [29].

For our measurements, we used absolute quantum yield technique, because all samples (nanoparticles, RE-doped glasses/fibers) absorb at 980 nm and belong to high scattering media.

4.1 QY measurement setup

The QY measurement setup is shown schematically in Fig. 14. It consists of the following parts: an integrating sphere, a laser diode as a pump source and a sample holder with an analyzed sample, a spectrometer, a multimode fiber, which collects the light from the sphere and directs it to the spectrometer and a computer with software performing the measurement data collection. The photograph of the actual laboratory setup is depicted in Fig. 15.

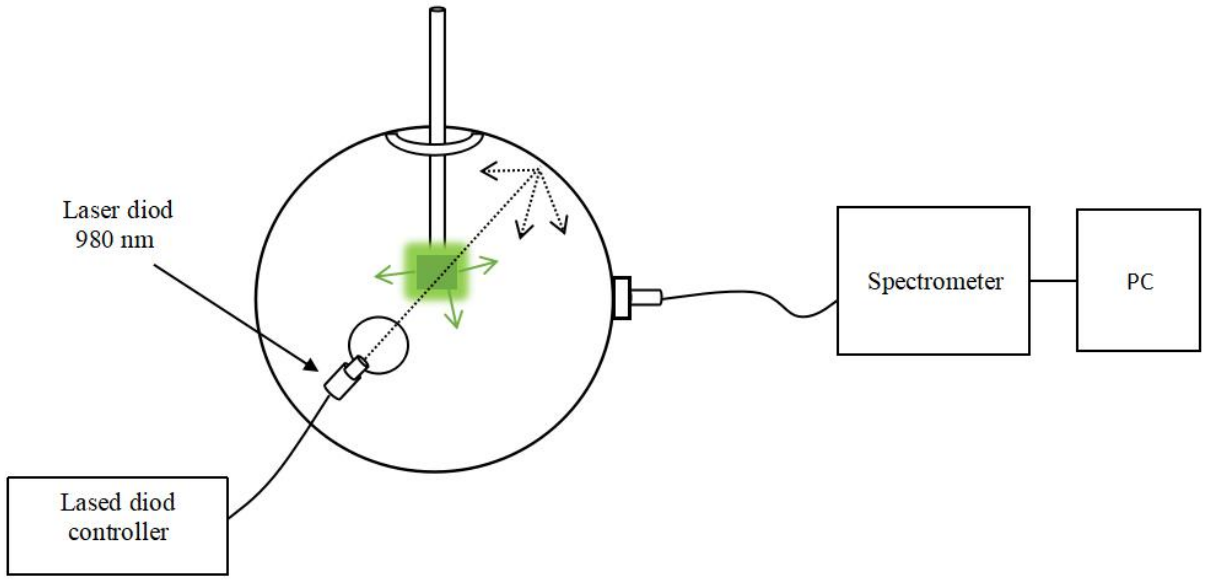

Figure 14. Schematic representation of QY measurement setup.

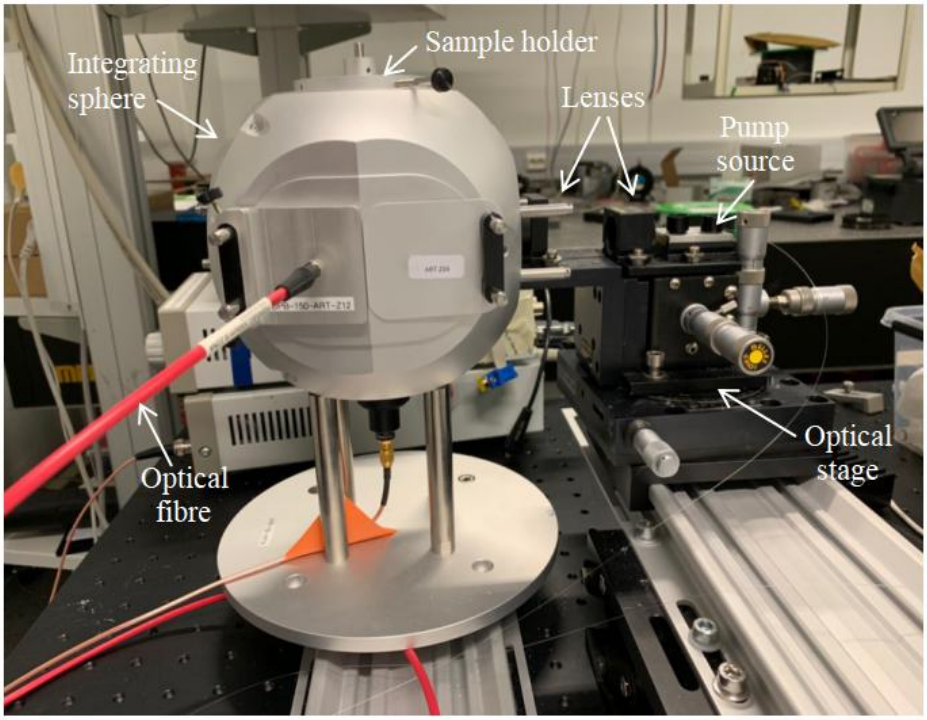

Figure 15. Photograph of the laboratory equipment for QY measurements.

Since up-conversion phosphors are highly scattering media, it make the light collection procedure quite complicated. Therefore, the practical solution is to perform the measurements by an integrating sphere.

An integration sphere is a hollow spherical cavity, the inner surface of which is a non-selective diffuse reflector. The operation principle of the integrating sphere is that the light entering the sphere through the input port experiences multiple diffuse reflections and is uniformly distributed in the internal volume of the sphere (Fig. 16). The detector or coupling fiber is placed at an angle of 90 degrees relative to the input port.

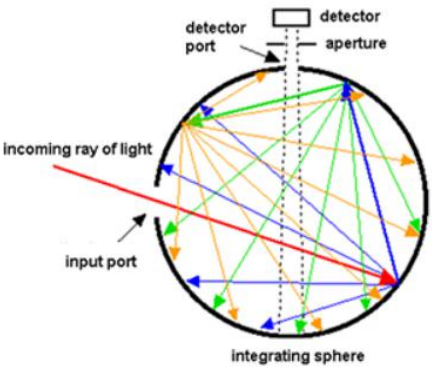

Figure 16. Optical rays reflection in the integrating sphere

In the measurement setup, we explored a precision integrating sphere UPB-150-ART from Gigahertz-Optik (Germany) with 150 mm diameter (Fig. 17). The sphere is made of a solid aluminum block, which provides very precise alignment of the measuring ports relative to each other. The port for the sample holder is located on the top of the sphere. The sampler holder is adjusted so to place the sample in the center of the integrating sphere. This position allows obtaining the uniformity of the scattered light distribution. The sample holder has the fixing blocks for a cuvette and for the glass/fiber samples. Four more input ports are situated along the equator of the sphere. One of the input port is used for the pump light launching, another for emitting light collection. Two others are blocked by the reflective covers. The sphere is based on the four holders with a common basement. This architecture allows to achieve high stability of the system and minimize the effect of the environmental perturbations.

Figure 17. General and inside view of the UPB-150-ARTA integrating sphere [30].

The inside surface of the UPB-150-ARTA integrating sphere is coated by Gigahertz-Optik‘s self-manufactured diffusely reflective barium sulfate (ODP97) coating, the reflection coefficient of which in the visible part of the spectrum is about 98.5% (Fig. 18). The coating contains 10 layers of barium sulfate, which ensures highly uniform reflective properties.

Figure 18. Spectral reflection of the integrating sphere coating [30].

As a pump source, a commercial wavelength- and power-stabilized laser diode Oclaro LC96X76P-20R with 980 nm central wavelength and operating in CW mode was used. The laser diode had a single-mode fiber pigtail with integrated low-reflection fiber Bragg grating maintaining the wavelength stability and output spectrum width. The fiber has a core/cladding parameters equaled to 4.5/125 μm, the mode-field diameter was 6 μm, and numerical aperture 0.16. The spectrum of the pump laser measured by the spectrometer through the integrating sphere is presented in Fig. 19. The laser source delivered 20 mW of the output power.

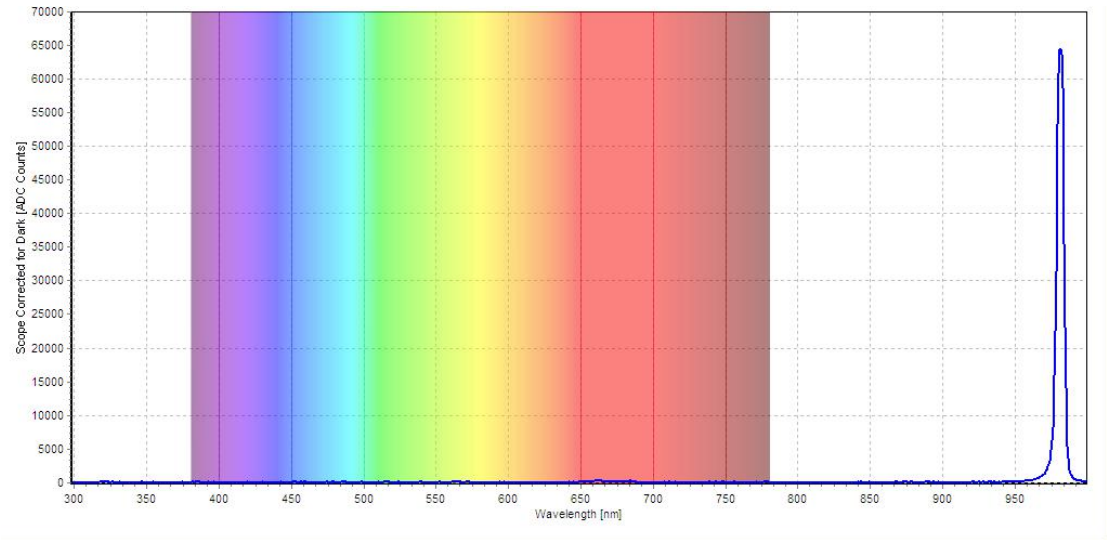

Figure 19. Spectrum of the pump laser diode.

The pump light was coupled to the sphere via the two-lens system (Fig. 20). The fiber pigtail of the source ensured the single-mode operation and uniformity of the launched

beam. The end of the fiber is placed on the fiber groove on the optical stage. First light is collimated by the lens with 4.5 mm of focal length and 0.47 numerical aperture. Higher than fiber numerical aperture of the lens guaranteed the good light collection from the fiber. Relatively short focal length in its turn helped to obtain a well-collimated beam. The second lens in the system played the focuser role. It had a 75 mm focal length, which allowed to obtain the focal point in the center of the integrating sphere. The power density of the pump light the sample plane was 63.7 W/cm^2.

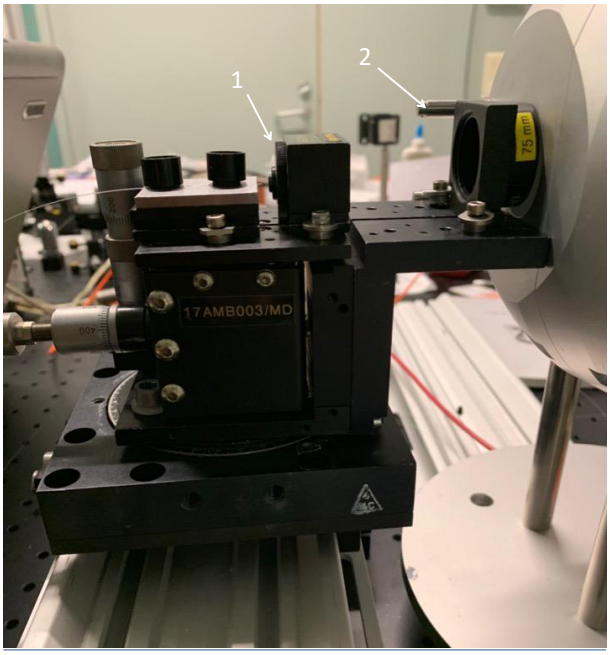

Figure 20. Pump light coupling via the two-lens system: 1) collimating and 2) focusing lenses.

AvaSpec-UV/VIS/NIR Broadband Spectrometer was used to measure the spectral characteristics of the samples. The spectrometer can operate in two wavelength ranges: 200-1100 nm and 950-1700 nm. This allowed to measure the visible and NIR wavelength range including the pump source in each case, thereby, to perform up- or down-conversion measurements by one setup.

Multimode fiber with a core diameter of 550 μm (FC550UEC, Thorlabs) and 0.22 numerical aperture was used to collect the emission light from the sphere and transfer it to the spectrometer. A large core diameter of the fiber allowed to delivery enough level of the light for highly sensitive measurement, and to qualify the frequency conversion efficiency up to several thousandths of one percent.

4.2 QY measurement procedure

To qualify the QY of the measured samples accurately and reliably it is critical to follow the defined measurement procedure. This is due to the fact that QY value is calculating based on absorbed and emitted photons numbers. Inaccurately performed measurements will result in the errors in the QY values and give the wrong conclusions about the frequency conversion process has taken place in luminescence phosphors. The QY measurement procedure includes the following steps (Fig. 21):

1. To measure the calibration factor of the measurement setup. For this the spectrum of the stabilized broadband light source should be measured through the system and then normalized to the maximum value.
2. To measure the reference spectrum. The pump spectrum is measured via the empty integrating sphere. The output power of the source should be fixed for the all other measurements.
3. To measure the spectrum of emission (direct excitation). The sample is placed in the center of the sphere using a specified holder in such a way, that it directly in the path of the excited incident light. The pump light should not heat the holder to avoid uncontrolled light scattering and reflection. Once the sample is fixed in the sphere, it is important to ensure that all unused ports are closed by reflective covers. The emission spectrum is collected.
4. To measure the spectrum of the scattered light (indirect excitation). The pump light is deflected from the sample by about 4 degrees and pointed to the sphere wall avoiding direct excitement of the sample. The scattered light spectrum is collected. The accuracy of the measurements is strongly depended on the re-excitation factor. The pump light reflected by the phosphor sample will be diffused in the sphere resulting in multiple secondary re-excitation. To determine the quantum yield, the only primary excitation must be taken into account. To avoid measurement error, the value of the sample re-excitation should be substracted from the direct emission.
5. The quantum yield is calculated by the Eq. 7.

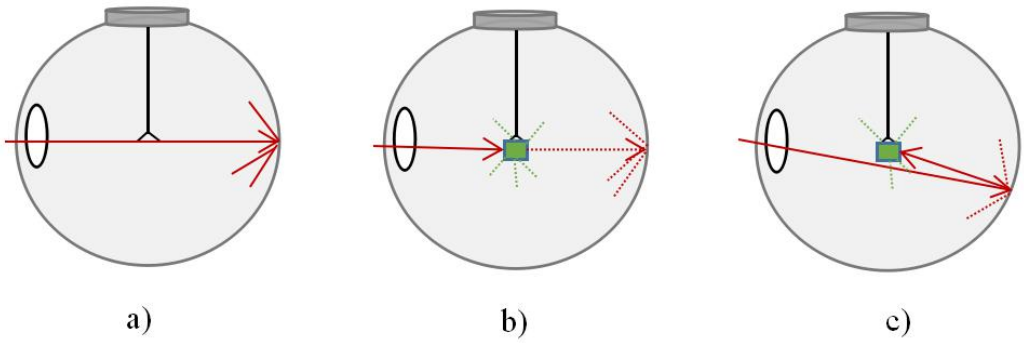

Figure 21. Illustration of the QY measurement procedure: a) pump light measurement without sample, direct (b) and indirect (c) excitation of the sample.

4.3 Measurement setup calibration

The calibration of QY measurement setup was started by the evaluation of the calibration coefficient (*k* from the Eq. 7). Due to the fact that the excitation and emission regions for the samples are usually well separated, the wavelength dependence of the system plays a crucial role in the measurement. Therefore, the directly measured values required an appropriate adjustment by the calibration factor. For this purpose, Thorlabs' Stabilized Tungsten-Halogen Light Source with radiation spectrum between 360-2600 nm was directed into an empty sphere using 400 µm fiber. The light was collected by a multimode fiber used for the QY measurement. The resulting spectrum from white light source measured by the spectrometer is shown in Figure 22. The calibration coefficients for each wavelength were calculated assuming that k=1 is corresponding to the absolute maximum of the spectrum.

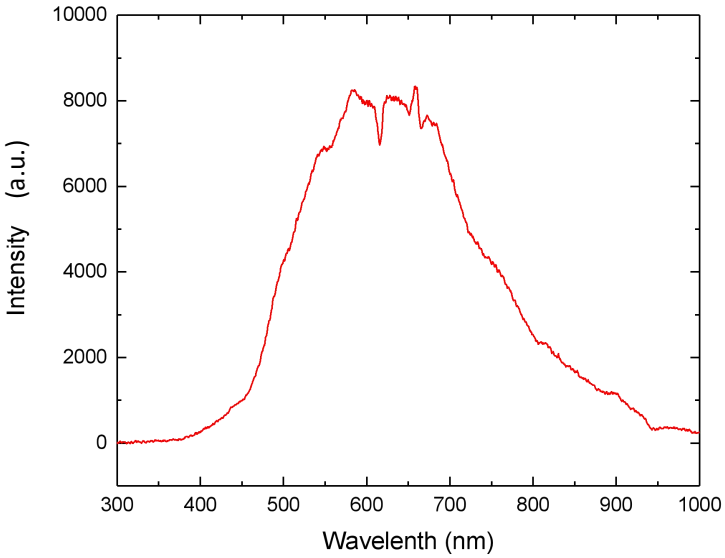

Figure 22. The spectrum of the white light source measured by the QY measurement setup.

The QY measurement setup was calibrated by the measurements of two commercial luminescence standards Acridine Orange fluorescent dye (QY=0.2) [31] and ZnCdSeS alloyed quantum dots (QY=0.8) [32]. This is a necessary procedure to verify the operation of the entire system, as well as to check the accuracy of the setup and identify the factors contributing to the errors. For the calibration measurement, Acridine Orange fluorescent dye was dissolved in ethanol, and ZnCdSeS alloyed quantum dots in hexane. The prepared solutions of both standards are shown in Fig. 23.

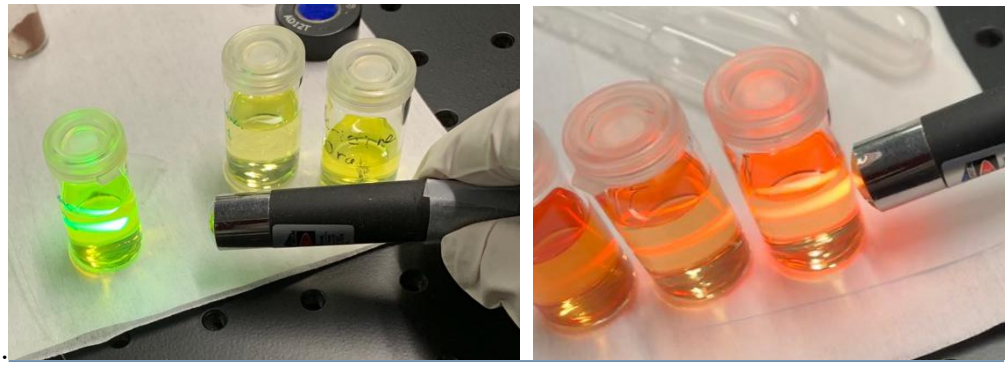

Figure 23. The luminescence of Acridine Orange dye (left) and ZnCdSeS quantum dots (right) solutions.

To perform the calibration measurement, the procedure described in section 4.2 was employed. The measurement of the reference spectrum was carried with the empty glass cuvette fixed in the sample-holder and placed inside the sphere. This was done to substrate the scattering of the pump light from the cuvette walls. For measurement of the emitted spectrum, the same cuvette was filled by the analyzed solution and placed back in the sphere. The emission spectrum with indirect excitation was collected by deflecting the pump light to the sphere wall. The resulting spectrum is presented in Fig. 24. At first, the laser pointer illuminating at the wavelength of 405 nm was used as a pump source, but due to the fact that the spectrum of the pointer was narrower than the resolution of the spectrometer, the estimation of the absorbed pump photons was not correct. Therefore, it was decided to use a laser diode (L405P20 Thorlabs) with a wider spectrum illuminated at the same wavelength.

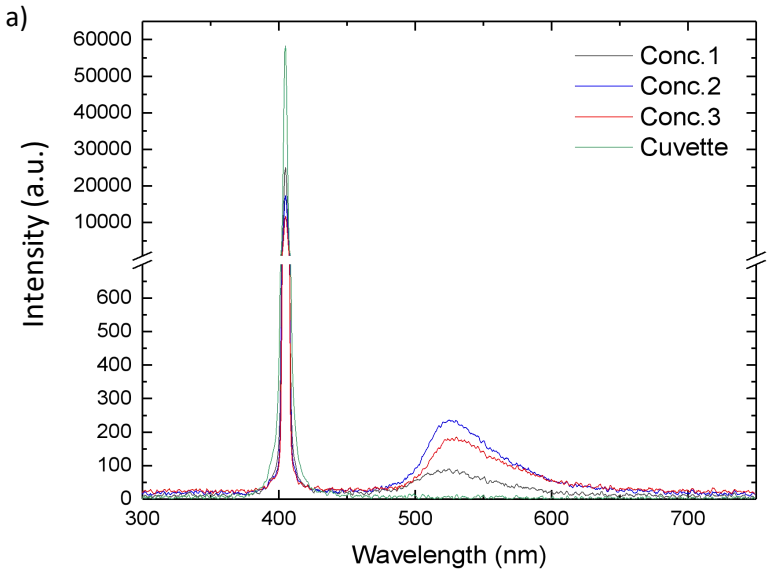

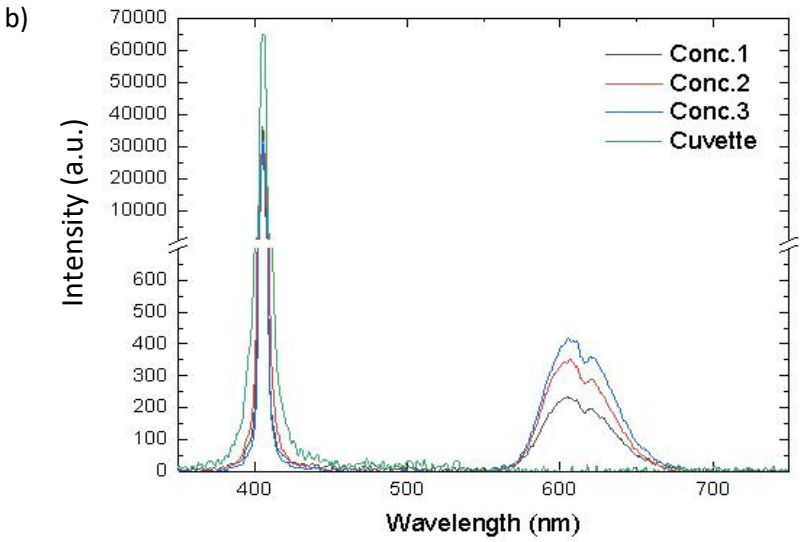

Figure 24. Reference and emission spectra of the Acridine Orange dye (a) and ZnCdSeS quantum dots (b).

For both samples, three solutions were prepared with a concentration of 1:2:3, where the first solution was too diluted according to the literature recommendation, the second was optimum, the third is too concentrated. To avoid the effect of the precipitation, the measurements were carried out with fresh solutions. The emission of Acridine Orange occurred at a wavelength of 525 nm and the emission of ZnCdSeS quantum dots at a wavelength of 610 nm, which corresponded to the standard values (Fig. 24). The measured quantum yield values for three different concentrations of Acridine Orange, from lowest to the most concentrated, was equalled to 0.15, 0.2, 0.22, which means that sample content in the first solution is insufficient, and the last one is saturated. The same measurements were carried out for three solutions of ZnCdSeS, and the following values of quantum efficiency were obtained: 0.76, 0.80, 0.83. Thus, the obtaining values of QY for the optimum concentration corresponds to the standard values, which means that the system is qualified for the QY measurements.

The next section will summarize the main factors affecting the QY measurement.

4.4 Critical issues of QY measurements

During the calibration procedure, the following issues have been identified as critical, which affects strongly the measurement accuracy and may result in the error of QY estimation.

Wavelength dependence of the setup components

The components of the setup such as internal surface reflectance of the integrating sphere, a delivered fiber and a spectrometer have wavelength-dependent characteristics. This dependence plays a crucial role in the evaluation of the emitted and absorbed photons numbers and might result in the significant error. Therefore, it is essential to take it into account for all measurements by means of the calibration coefficient *k*.

The lens coupling system.

It is necessary to focus the beam to the sample plane to obtain the sufficient excitation fluency. This is possible by choosing a lens with an appropriate focal length.

Pumping source

The excitation source must be highly stable in terms of wavelength and output power. Its spectrum width should not be narrower than the resolution of the spectrometer.

Separation of Emission and Excitation bands

For the accurate QY evaluation, it is necessary to separate the emission and excitation regions of the spectrum accurately to avoid the error in the calculation of the emitted and absorbed photons.

External light

To perform highly sensitive measurement of the QY, the ground noise, what is the light from the ceiling lamps or the laboratory devices, should be eliminated. Therefore, it is better to carry out the measurements by placing the setup in black-wall closure.

5. QY MEASUREMENTS IN LUMINESCENCE MATERIALS

The QY measurements were performed for several types of luminescence samples: upconversion nanoparticles, upconversion nanoparticles-doped glasses, rare-earth-ions-doped glasses. All samples were in solid crystalline form and exhibited strong light scattering. They are characterized by different host matrixes and/or different concentration of the rare-earth dopants. The QY measurement procedure fully coincided with the one described in Section 4.2. The wavelength of excitation was 980 nm from the laser diode (Fig. 19).

5.1 Upconversion nanoparticles

Three samples of UCNPs, all doped by Yb (sensitizer) and Er (activator) ions, were investigated. The samples were primarily distinguished by the host matrix composition ($NaYF_4$, Y_2O_3, LaF_3), which phonon energy varied from 300 to 550 cm^{-1}.

The nanoparticles in the form of powder were placed on the transparent glass substrate using double-sided tape, fixed in the sample's clips-holder, and then located in the center of the sphere.

Upconversion nanoparticles $NaYF_4$:Yb,Er

The UCNPs sample was provided by University of Turku, Finland. Nanoparticles were synthesized by the modified thermal coprecipitation method. For a synthesis of NPs, the methanol solutions of RE chlorides with oleic acid and octadecene was heated at 160 °C for 40 min and then cooled down to the room temperature to form the rare earth-oleate complex. Then, methanol solution of NH_4F and NaOH were added to the solution and stirred for 30 min without argon to evaporate the methanol and to ensure that all of the fluorides were consumed completely. The solution was subsequently heated up to 310ºC in an argon atmosphere for 90 min and cooled down. The formed nanoparticles were precipitated by the addition of ethanol to the reaction solution. To separate obtained NPs, the solution was centrifuged for 8 min [33].

The reference spectrum of the pump source and the emission spectra of the UCNPs for direct and indirect excitations measured for the QY evaluation are presented in Fig. 25. In order to re-evaluate the accuracy and reliability of the measurements, five consecutive records of the emission spectra under the same conditions were performed (inset Fig. 25). A pause of 10 s was set between the measurements to avoid the particles heating by pump light. A series of measurements demonstrated the absolute identity of the emission spectra, which was a sign of high system reliability.

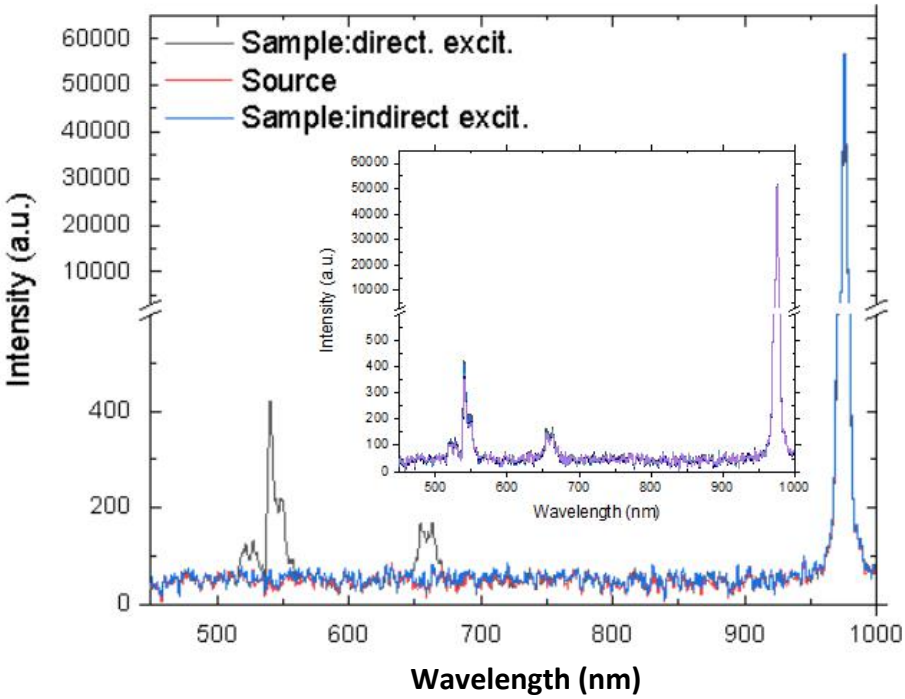

Figure 25. The reference spectrum of the pump source ("Source") and the emission spectra of $NaYF_4$:Yb,Er UCNPs for direct and indirect excitations. In the inset: five consecutive measurements of the emission spectra with 10 s pause between the sets.

Under 980 nm pump, the nanoparticles exhibited the upconversion luminescence at the wavelength ranges around 530 and 660 nm. The green emission band consists of two partially overlapped emissions at 522 and 540 nm. This is the result from the fact that first, the population of the $^4F_{7/2}$ level in Er ion occur, then an intermediate non-radiative relaxation to the levels $^2H_{11/2}$ and $^4S_{3/2}$ takes place, and then the radiative relaxation to the $^4I_{15/2}$ level finish the energy transfer process. Also, the red emission is observed at 660 nm during the transition from the $^4F_{9/2}$ level to $^4I_{15/2}$, due to partial non-radiative relaxation

from the $^4F_{7/2}$ level to $^4F_{9/2}$. The energy diagram of these processes is presented in Figure 26.

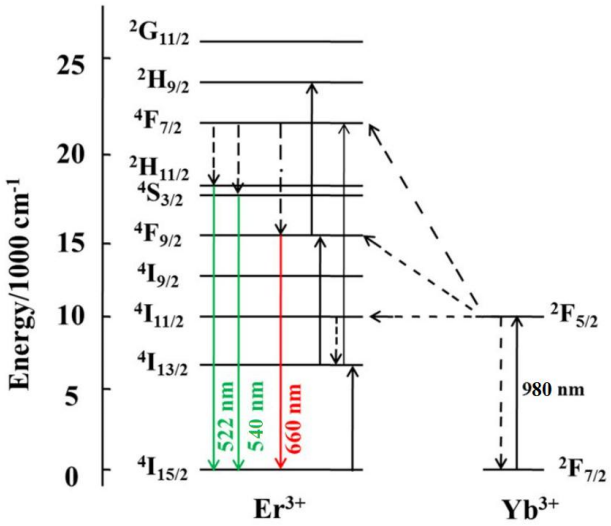

Figure 26. Energy level diagram of UC process in Er Yb.

The resulting quantum yield for $NaYF_4$:Yb,Er UCNPs is 0.6%. Despite the small absolute value, this is good QY result for the current UCNPs technology. The theoretical value of the up-conversion quantum yield cannot exceed 50% for two-photon absorption process, but in case of nanoparticles, due to inhomogeneity and strong surface quenching effect, it rarely exceeds 1-2% [8].

Upconversion nanoparticles Y_2O_3:Er,Yb

The second type of UCNPs (PTIR660/UF) was synthesized by Phosphor Technology Ltd. (Stevenage, England). The percentage of lanthanides, as well as the method and parameters of the synthesis are the trade secret of the manufacturer. The pump reference spectrum and the emission spectra for the direct and indirect excitations are presented in Figure 27. These nanoparticles exhibited the upconversion luminescence at the red wavelength only of the visible spectrum range. The red emission peaks arise from $^4F_{9/2} \rightarrow {}^4I_{15/2}$ level transition corresponding to 660, 675, 687 nm emissions. In contrary to the first UCNPs, there was no green emission detected in Y_2O_3:Er,Yb sample.
The up-conversion QY of the Y2O3:Yb,Er UCNPs is 0.46%.

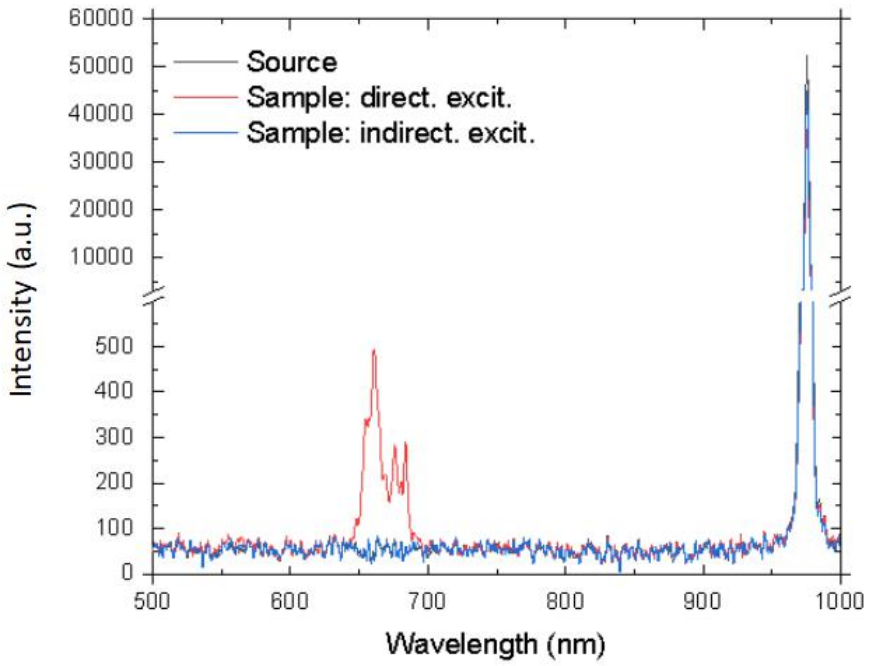

Figure 27.The reference spectrum of the pump source ("Source") and the emission spectra of Y_2O_3:Yb,Er UCNPs for direct and indirect excitations.

Upconversion nanoparticles LaF_3:Er,Yb

The third sample of UCNPs was a solution of separate nanoparticles made of LaF_3 and doped by Yb and Er ions. To avoid the clustering effect, these nanoparticles were covered by PVP (Polyvinylpyrrolidone, water-soluble polymer used as nanoparticles dispersant). A drop of the particles solution was placed on a glass substrate and dried. The nanoparticles luminescence was extremely weak, so it was impossible to measure the emission. The reason could be a strong surface quenching effect at the border of nanoparticles' host matrix and polymer coating. As the next step, the nanoparticles sample was ablated by high power 980 nm multimode laser to burn the PVP shell. This procedure helped to improve the emission efficiency a little bit, however, it was not enough to perform the reliable measurement. The spectrum of the nanoparticles upconversion luminescence is shown in Fig. 28. There was a very small peak of the red emission at 640 nm.

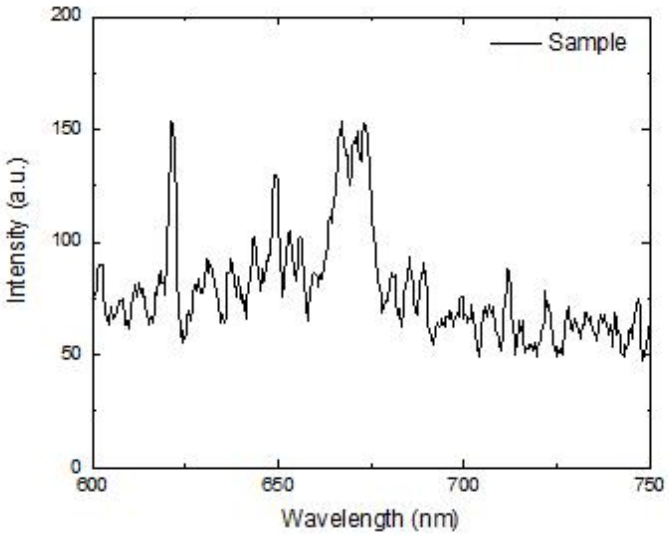

Figure 28. UC spectrum of LaF_3:Er, Yb UCNPs

The QY measurement results of UCNPs are summarized in Table 3. The strongest upconversion was demonstrated by the sample with $NaYF_4$ matrix. This matrix is characterized by one of the lowest value of the phonon energy. However, the structure homogeneity and possibly OH (water) species vibration could be a reason of low efficiency of the frequency conversion process. The sample with Y_2O_3 demonstrated lower QY value comparing to the sample with $NaYF_4$. This might be a result of higher phonon energy (~550 cm^{-1}). Also, it might be due to the lower concentration of the dopants, which impossible to compare due to the absence of the exact composition information. Usually, Y_2O_3-based nanoparticles are produced by "dry" technique such as a bombarding of the target, so the impact of OH species is unlikely. From another side, the structure homogeneity might be a critical issue. Despite on the fact that LaF_3 matrix is characterized by very low phonon energy (~300 cm^{-1}), the efficient upconversion emission was not observed in these type of nanoparticles due to the strong impact of the surface and water quenching effects.

As a common observation for all UCNPs samples, there was no detected emission in NIR wavelength range, therefore, the down-conversion as a competitive process is not manifested in these nanoparticles.

Sample	Doping ions	Matrix, phonon energy cm^{-1}	UC, %	DC,%
UCNPs 1.	Er^{3+},Yb^{3+}	NaYF4, 350	0.6	No
UCNPs 2.	Er^{3+},Yb^{3+}	Y2O3:Yb,Er, 550	0.46	No
UCNPs 3.	Er^{3+},Yb^{3+}	LaF3, ~300	-	-

Table 3. The results of QY measurements of UCNPs.

5.2 RE- and upconversion nanoparticles-doped phosphate glasses

As it was discussed in Section 3.2.2, the phonon energy of the host matrix has a significant impact on the efficiency of the upconversion process. Therefore, to minimize the undesired non-radiative relaxation due to the lattice vibration, the active centers are surrounded by the environment with low phonon energy. In this means, the traditional glasses are interior to inorganic material as the host media (see Table 2.). From another side, the glasses/fibers are highly suitable for the gain media of the lasers. To overcome the disadvantages of the glasses in potential coherent sources for visible wavelength range, the technology is going towards to the integration of the UCNPs into the glass material, since the outer environment does not have primarily effect on the UC process, but instead, it acts as a light delivery medium.

To experimentally investigate the difference between UC efficiency in the glass medium doped by the ions and UCNPs, four samples of the doped phosphate glasses prepared at the Laboratory of Photonics, TAU were investigated. Two samples are doped by Er ions. Here, the glass acts as a host matrix. Two others were doped by NaYF4:Yb, Er UCNPs, which were described and investigated in Section 5.1. A type of glass was chosen due to its low melting temperature and stability against crystallization. Low melting temperature is essential to avoid the thermal degradation of the UCNPs. Stability against crystallization in its turn requires for structure homogeneity, which directly affects the losses. The photograph of the glass samples is presented in Figure 29. The investigation of these samples included both up- and down-conversion measurements.

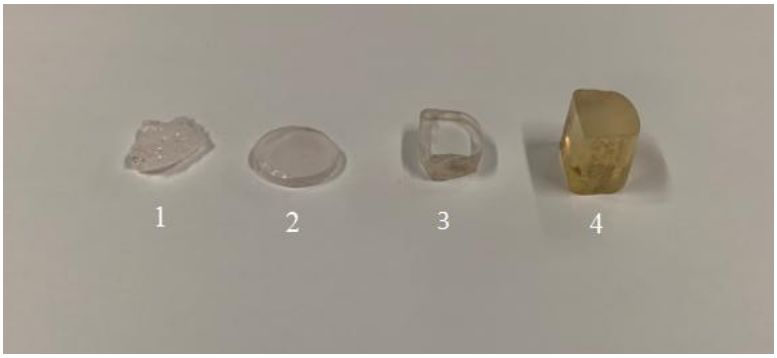

Figure 29. Phosphate glass samples doped by Er ions and UCNPs. The numeration on the photograph corresponds to the sample number: 1-P.1, 2-P.2, 3-P.3 and 4-P.4.

Er-doped phosphate glasses

The Er-doped glass samples P.1 and P.2 were fabricated by a melt-quenching technique. They have identical composition but distinguished by the heat treatment parameters. The $0.25Er_2O_3$ nanocrystals were mixed with $75NaPO_3$-$25CaF_2$ glass material, and then heat treated at the glass transition temperature 950ºC for 17 h in the air environment. The glass sample P.1 was additionally heated during 3h at the 20ºC above the crystallization peak temperature.

The emission spectra for up- and down-conversion processes are presented in Figure 30 for the glass sample P.1 and in Fig. 31 for the glass sample P.2.

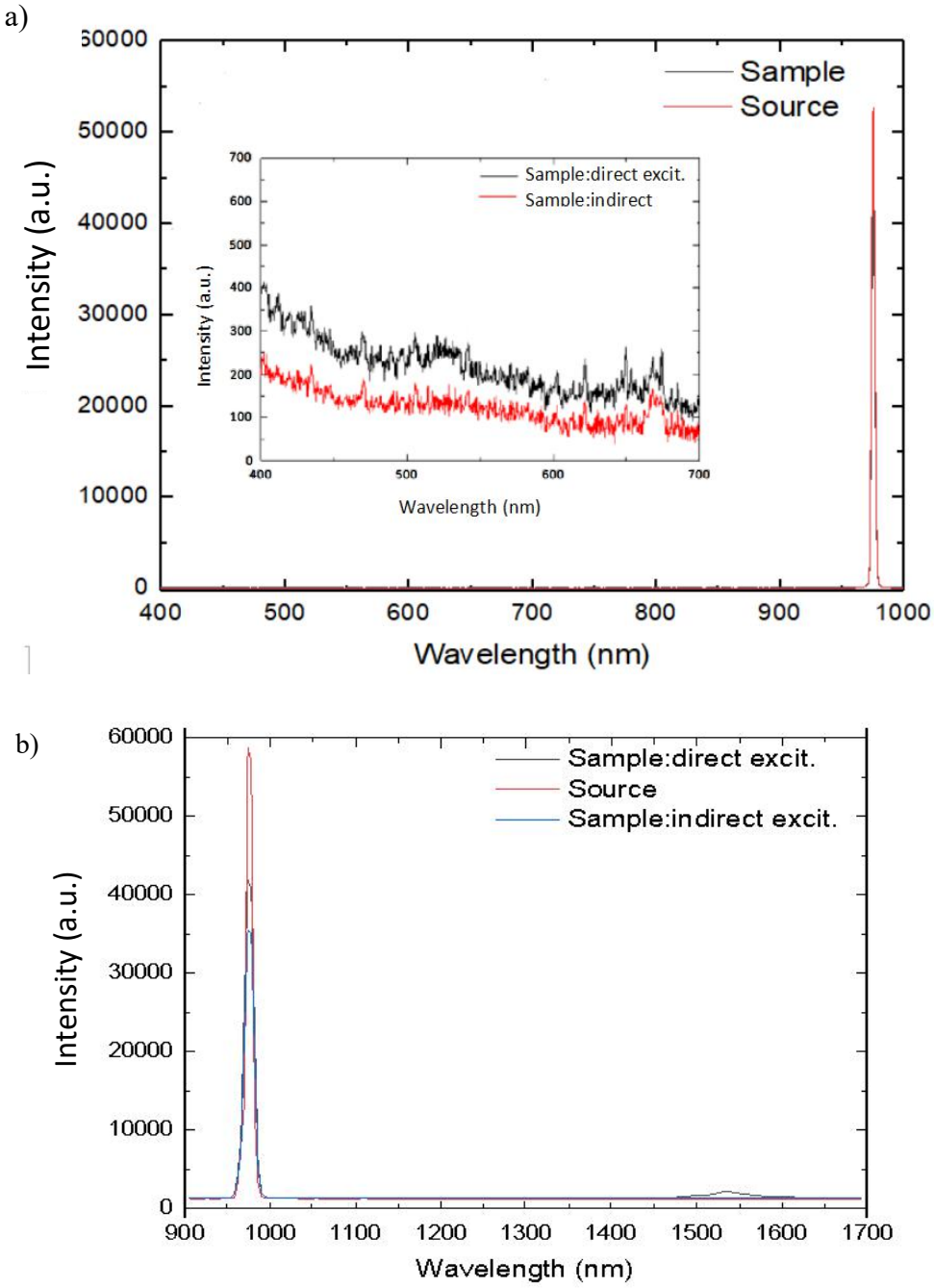

Figure 30. The reference of the pump source and emission spectra of the glass sample P.1. a) Upconversion, In the inset: the enlarged picture of the luminescence in the visible wavelength range. b) Down-conversion.

Both samples exhibited very weak green (520 nm) and red (670 nm) emissions, which are corresponding to the $^4H_{11/2} \rightarrow {}^4I_{15/2}$ and $^4F_{9/2} \rightarrow {}^4I_{15/2}$ transitions. Due to extremely low upconversion efficiency, it was impossible to evaluate the QY. In contrast to this, the down-conversion process was more pronounced as in the glass sample P.1, as in P.2. The peak around 1540 nm was clearly detected corresponding to the $^4I_{13/2}$ -$^4I_{15/2}$ level transition. Moreover, in the glass sample P.2 the intensity of the NIR emission was higher than in the

sample P.1. As a result, the QY values for the samples P.1 are P.2. are 58.18% and 75.3%, respectively. Since the QY values are lower than 100% the energy transfer process can be qualified as down-shifting.

As a consequence, the technological process for the fabrication of the sample P.2 was a little bit better in terms of NIR emission efficiency. But both samples demonstrated very low upconversion efficiency. This result is most probably due to the high phonon energy of the phosphate glass matrix (1200 cm^{-1}). Also, the absence of Yb ions could negatively affect UC efficiency, since this ion has higher absorption cross-section.

a)

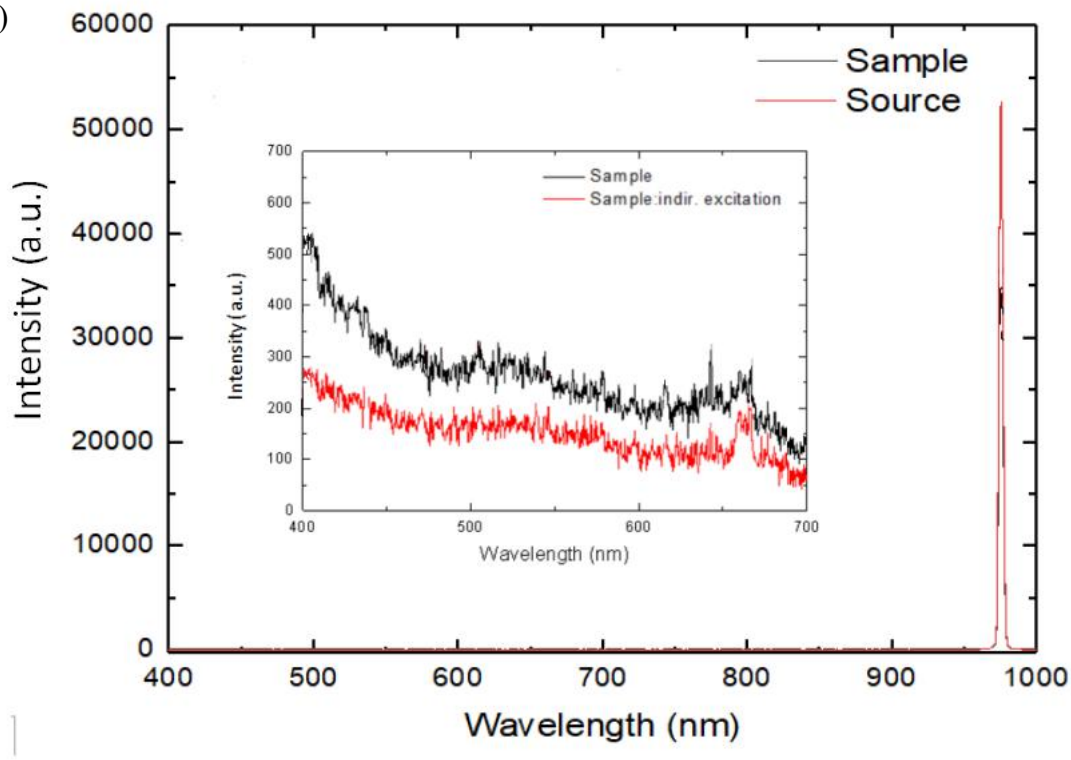

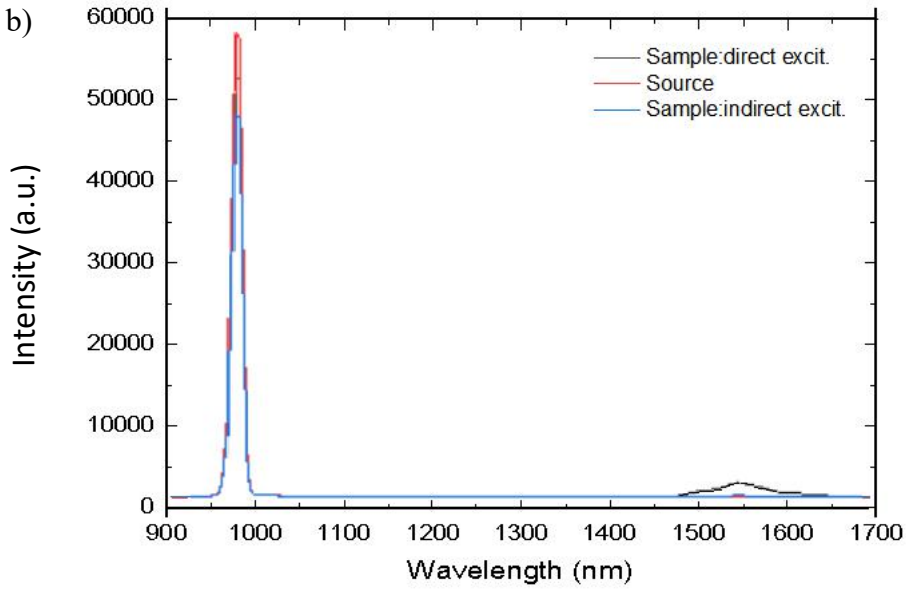

Figure 31. The reference of the pump source and emission spectra of the glass sample P.2. a) Upconversion, In the inset: the enlarged picture of the luminescence in the visible wavelength range. b) Down-conversion.

Upconversion nanoparticles-doped fluore-phosphate glasses

The UCNPs-doped glasses (Glass sample P.3 and Glass P.4) were fabricated by direct doping method, using the glass matrices with lower melting points than nanoparticles. The Glass P.3 was prepared by adding 5 wt% of the $NaYF_4:Er^{3+},Yb^{3+}$ nanocrystals into $90NaPO_3$-10NaF glass system, after melting it at 750 °C. To improve the dispersion of UCNPs in the glass, the melt was held for 3-5 min (dwell time) manually stirring at the same time. [34]

The reference spectrum of the pump source and the emission spectra of up- and down-conversion of glass P.3 are presented in Fig. 32.

a)

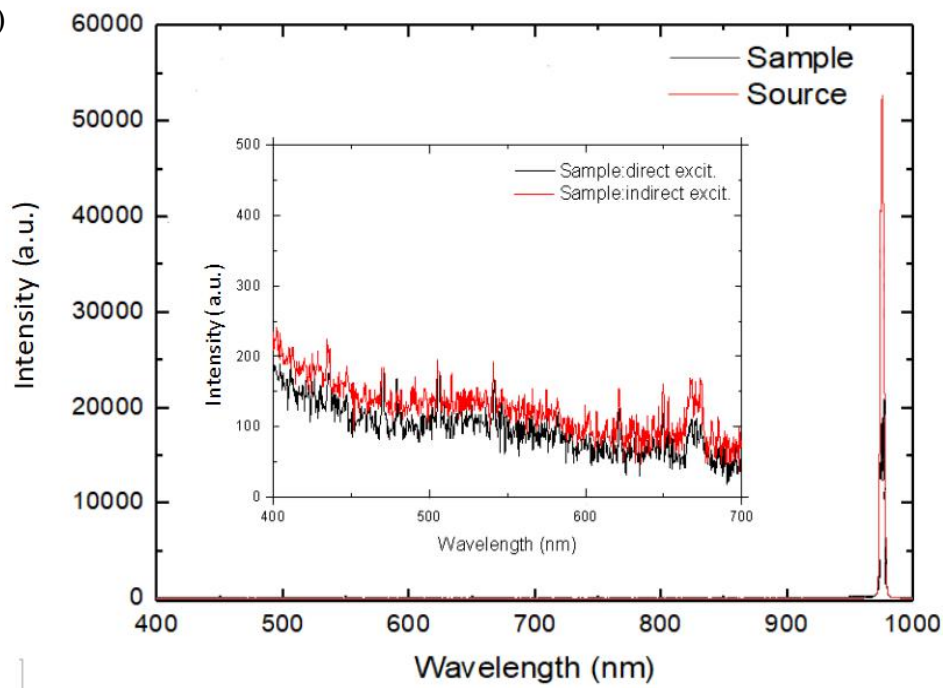

b)

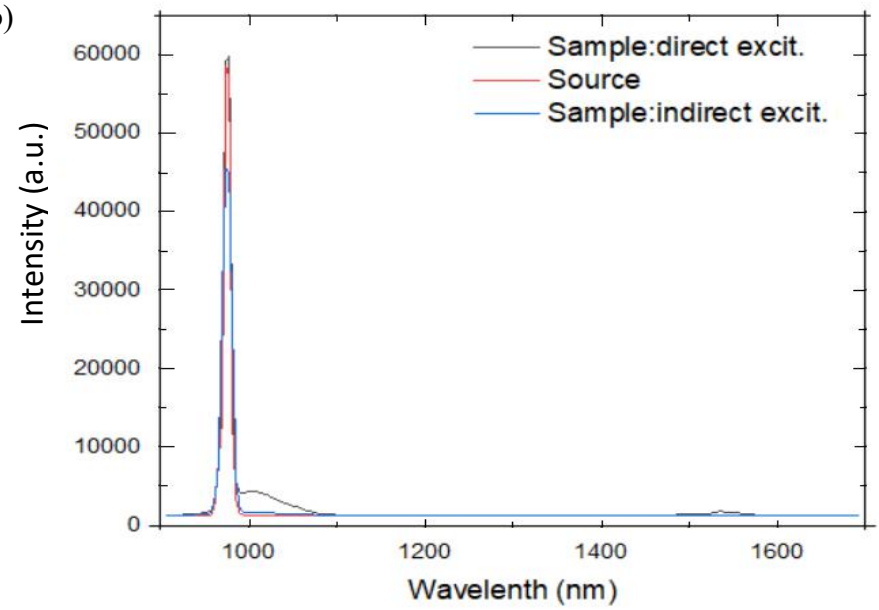

Figure 32. The reference of the pump source and emission spectra of the glass sample P.3. a) Upconversion, In the inset: the enlarged picture of the luminescence in the visible wavelength range. b) Down-conversion.

.

The very weak red UC emission was detected at 670 nm. The corresponding QY of the up-conversion is 0.002%. The down-conversion emission observed at 1540 nm was more pronounced in this sample as in the samples P.1 and P.2. However, its efficiency was much lower given only 15.3% of the QY. This is a very interesting result since the bare UCNPs did not exhibit any DC luminescence.

A decrease in the up-conversion efficiency in comparison to the bare nanoparticles appears most likely because of heating caused the corrosion of the nanocrystals or the change in their composition. In the case of uniform corrosion, the relative concentrations of the doping particles would remain the same, but their size would decrease, what will unavoidably lead to the decrease of UC intensity. This could relate to the non-radiative quenching through the border between the nanocrystals and the glass matrix, and the probability for such relaxation increasing with decreasing of nanocrystal size. In the phosphate glass matrix, the surface quenching is proceeded via multiphonon de-excitation due to the high phonon vibrations around 1200 cm^{-1}. [34]

The glass sample P.4 was also fabricated by direct doping method by adding 5 wt% of the $NaYF_4:Er^{3+},Yb^{3+}$ nanocrystals in $83.25NaPO_3$ – 9.25NaF – 5ZnO- $2.5Ag_2O$ glass system. The spectra of the reference and up- and down-conversion emission of the glass P.4 are presented in Figure 33.

a)

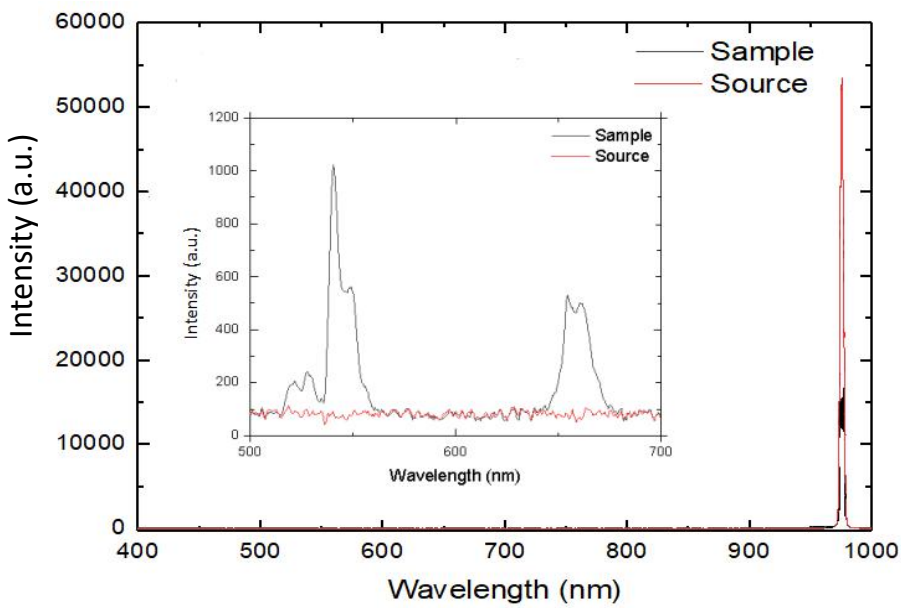

b)

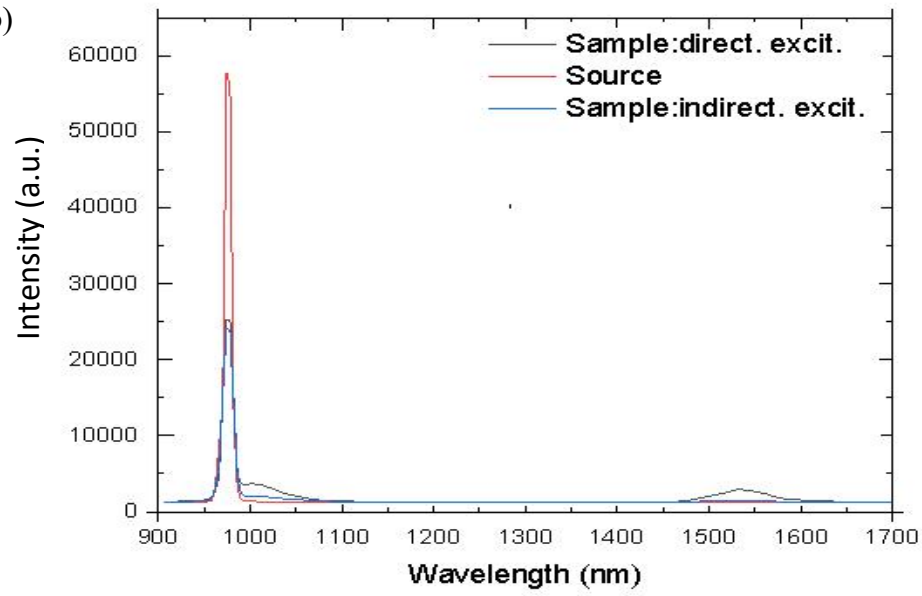

Figure 33. The reference of the pump source and emission spectra of the glass sample P.4. a) Upconversion, In the inset: the enlarged picture of the luminescence in the visible wavelength range. b) Down-conversion.

The sample demonstrated strong multi-wavelength green UC emission at 520 nm, 530nm ($^2H_{11/2}\rightarrow{}^4I_{15/2}$) and at 546 nm, 553 nm ($^4S_{3/2}\rightarrow{}^4I_{15/2}$). The red UC emission was observed at 662 nm and 673 nm ($^4F_{9/2}$ → $^4I_{15/2}$). The up-conversion QY is 0.43%. The value is smaller than for the bare UCNPs, but the overall decrease of the QY is not dramatic as for the sample P.3. This might be a result of nanoparticles crystal clumping and/or better homogeneity of the outer environment, as a consequence, a decrease of surface quenching. Also, this sample is additionally doped by silver nanoparticles. Confinement of excitation wavelength by metallic NPs contributes to a strong field enhancement through the excitation of the collective oscillation of electron clouds called localized surface plasmon (LSP). LSP enhances the confined electric field in the vicinity of Er^{3+} ions, which results in an increment in absorption by emitter ion (lightning rod effect) and radiative decay rate from the upper levels. Both of these consequences lead to the enhancement of UC emissions.[35] To get a clear understanding of the overall picture of the physical process inside the glass, the additional investigation is necessary.

IR DC emission from the glass P.4 is detected at wavelength 1540 nm ($^4I_{13/2}$ -$^4I_{15/2}$). The QY value is 21.77%, which means that the down-shifting effect is taken place.

The results of QY measurements for RE- and UCNPs-doped phosphate glasses are summarized in Table 4.

Sample	Dopants	Glass system	UC,%	DC,%
Glass P.1	$0.25Er_2O_3$	$75NaPO_3$-$25CaF_2$	-	58.18
Glass P.2	$0.25Er_2O_3$	75NaPO3-$25CaF_2$	-	75.3
Glass P.3	5wt% $NaYF_4$:Er^{3+},Yb^3	$90NaPO_3$-10NaF	0.002	15.3
Glass P.4	5wt% $NaYF_4$:Er^{3+},Yb^3	$83.25NaPO_3$–9.25NaF–5ZnO-$2.5Ag_2O$	0.43	21.77

Table 4. Results of phosphate glasses QY measurements.

5.3 RE-doped tellurite glasses

As it was demonstrated by the experiments from the previous sections, the UC efficiency strongly depended on phonon energy of the host matrix as well as it homogeneity. Therefore, in this section, the luminescence substances based on highly homogeneity host matrix with relatively low phonon energy were investigated. The homogeneity host matrix was tellurite glass doped by Er and Yb ions.

Altogether, five samples of tellurite glasses with different concentration of Yb, Er ions were analyzed. The samples were provided by Devyatykh Institute of Chemistry of High-Purity Substance of RAS, Russia. Tellurite glass system has advantages of higher glass transition and softening temperatures, higher stability against crystallization, and lower thermal expansion compare to other glasses. Additionally, the tellurite glass samples are characterized by extremely low content of OH- groups, which negatively influence the fluorescence.

The first three glasses (Glass T.1, Glass T.2, Glass T.3) were made of TeO_2-WO_3-La_2O_3-Bi_2O_3 glass matrix, doped by only Er^{3+} ions. They were produced by

melting the oxides batch inside a sealed silica chamber at a temperature of 800 °C in the atmosphere of purified oxygen. The Er_2O_3 was introduced at the stage of charge mixing. The synthesis of the glasses was carried out in platinum crucible for several hours with recurrent stirring of the melts, and then glasses were annealed at the transition temperature (~400 °C). Due to the specific drying technique, the low content of hydroxyl groups (0.005 cm^{-1} - 0.018 cm^{-1}) was achieved. [36]

The others two glass samples (Glass T.4 and Glass T.5) were made of TeO_2–ZnO–La_2O_3–Na_2O glass matrix, doped by Er^{3+} and Yb^{3+} ions. TeO_2 – ZnO -based glasses were produced by gas-phase deposition of oxides from the vapors of organo-metallic compounds in the flame of the hydrogen-oxygen burner. [37] The glass samples are also characterized by the low content of OH species (0.006 and 0.028 cm^{-1}).
The details of the glass composition for all samples are presented in Table 5.

The UC and DC spectra for the tellurite glass samples are depicted in Fig. 34. The green and red UC emissions were observed at 560nm ($^4S_{3/2}\rightarrow{}^4I_{15/2}$) and 670 nm ($^4S_{3/2}\rightarrow{}^4I_{15/2}$), correspondingly for all samples. Notably, green emission was always dominated. However, the intensities of the peaks varied significantly between the samples. The sample T.1 demonstrated the smallest UC emission, and the QY was only 0.064%. Relatively low efficiency could be explained by the fact that the optimum concentration of the ions was exceeded (4%) and concentration quenching occurs. The samples with lower concentration exhibited better UC efficiency over 1% value for 1.34 % of Er ions content. The variation of hydroxyl group concentration between the samples should not influence on the upconversion process because the absolute value is extremely low.

The sample T.5 had the strongest green and red emissions and the highest value of QY equalled to 3.3%. In contrast, the sample T.4 demonstrated much lower efficiency of UC process corresponding to 0.38% of the QY. This might be the result of low concentration for both Yb and Er ions, and as a consequence, the energy transfer between the ions was not efficient. The sample T.5 has almost four times higher concentration of Yb ions, resulting in the increase of the UC efficiency by the order of magnitude.

The NIR down-conversion was observed for the wavelength range 1540-1600 nm where the highest concentration of Er ions in the glass resulted expectedly in the longer emission wavelength. The sample T.4 and T.5 also demonstrated an additional parasitic emission band around 1000 nm corresponding to the transition between the energy levels of Yb ions. Despite on the valuable difference of the Er ions concentration in the samples, the intensities for the emission around 1550 nm are quite identical (Fig. 34b), what could give expectation in similar QY values. However, they are varied significantly. The samples T.1, T.4, and T.5 have QY below 100% (Table 5), which means that the NIR emission is a result of the down-shifting effect. In contrary, the sample T.2 and T.3 have QY more than 100%. This is a sign of down-conversion process, where one absorbed photon with high energy results in the emission of two photons with lower energy. If two emitted photons are identical, then QY should be equal to 200%. However, when two photons are characterized by different energies, then the QY value is between 100 and 200%. According to the energy conservation principle, one photon should be at the wavelength 1550 nm, and the second is around 2700 nm, which fully coincides with the luminescence properties of the glass described in [36].

a)

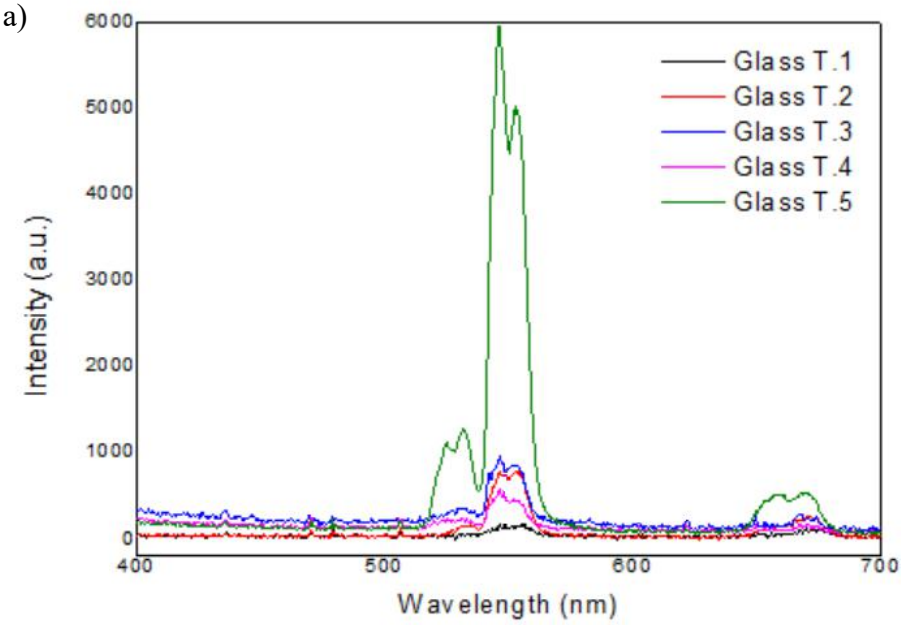

b)

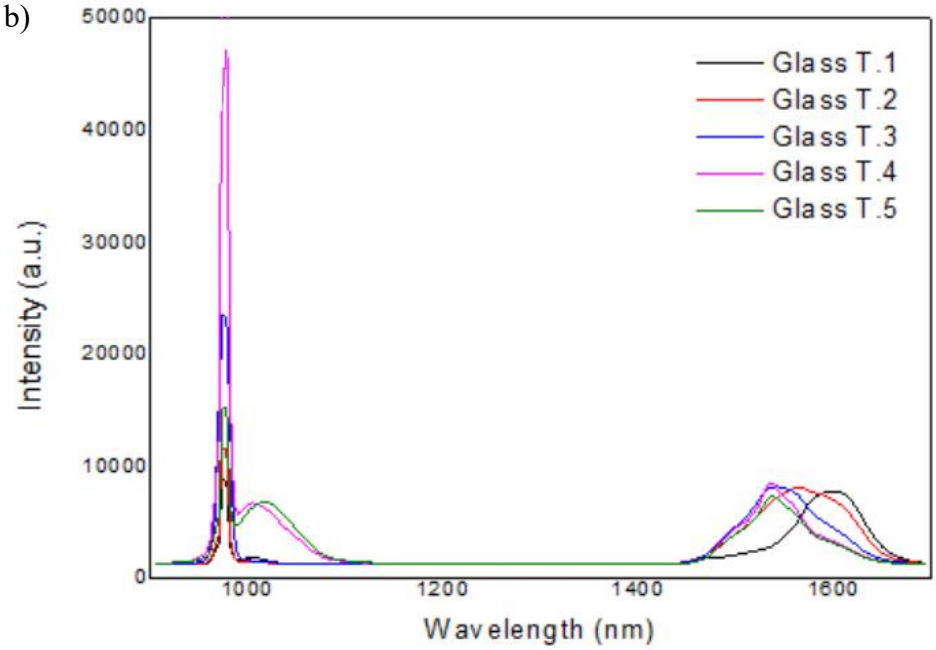

Figure 34. Up- (a) and down-conversion (b) spectra of emission from the tellurite glasses.

The Raman spectra were measured to evaluate the phonon energies of the tellurite glasses, the presence of the hydroxyl group, and the structural homogeneity of the glasses. The measurement results are presented in Figure 35. The phonon energy of the samples is varied between 750 to 920 cm^{-1}. The relatively higher phonon energy in the sample T.2 (~920 cm^{-1}) could be an explanation of less well performance in comparison to the sample T.3 (~750 cm^{-1}) (Table 5).

No peak in the range 1000-4000 cm^{-1} was detected. This is a confirmation of the high homogeneity of the structure and extremely low hydroxyl group concentration. The "water-free" samples do not suffer from OH-quenching effect, which would negatively affect 2700 nm wavelength emission due to the overlapping of the OH absorption and Er emission at this wavelength. As a consequence, the down-conversion process with the emission of two different photons can be observed. The homogeneity of the host structure positively affect the upconversion emission, however, the concentration of the active centers play a valuable role too.

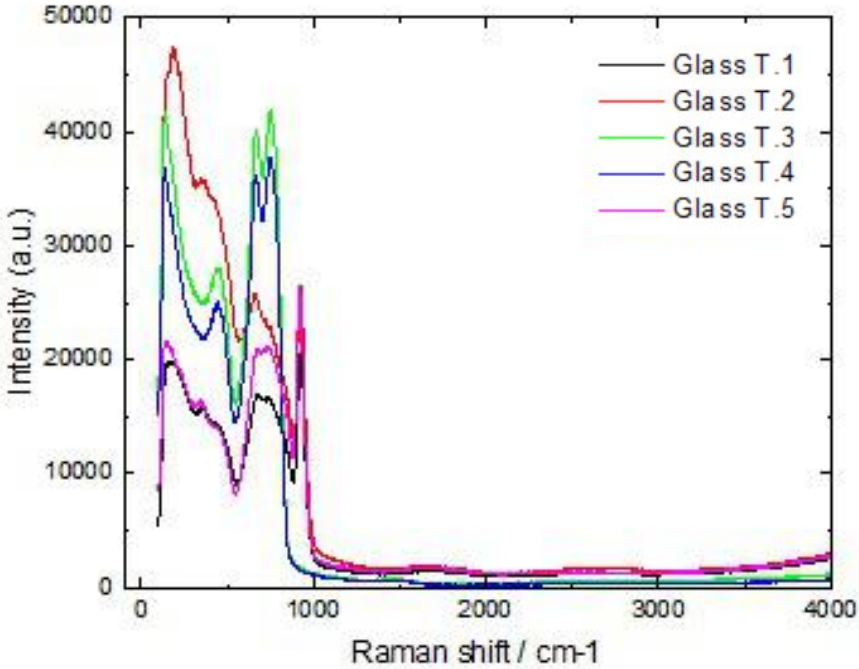

Figure 35. Raman spectra of the tellurite glass samples.

The results of the glasses QY measurements are summarized in the Table 5.

Sample	Dopant concentration	OH^-	UC,%	DC,%
Glass T.1.	Er_2O_3 - 4%	0.018 cm^{-1}	0.064	61
Glass T.2.	Er_2O_3 - 1.34%	0.005 cm^{-1}	1.1	120.4
Glass T.3.	Er_2O_3 - 0.42%	0.006 cm^{-1}	0.97	154
Glass T.4.	Er_2O_3-0,1% Yb_2O_3-0,1%	0.028 cm^{-1}	0.38	42.8
Glass T.5.	Er_2O_3-0,1%, Yb_2O_3-0,45%	0,021 cm^{-1}	3.3	52.6

Table 5. Results of the QY measurements for the tellurite glasses.

6. CONCLUSIONS

In this thesis, the influence of the host matrix on the upconversion efficiency in the luminescence materials was investigated. The samples under consideration were the upconversion nanoparticles with fluoride and oxide matrixes, phosphate glasses doped by upconversion nanoparticles and rare-earth dopants, and tellurite glasses doped by Er/Yb,Er ions. Special attention was paid to phonon energy of the host material, surface and water quenching effects, material homogeneity, dopants concentration, down-conversion as a competitive process. The quantum yield was chosen as a measure of luminescence efficiency.

To quantify the quantum yield, a reliable and sensitive measurement setup was built. The setup is based on an integrating sphere and broadband spectrometer, and capable to operate in the visible and near-infrared wavelength range from 300 to 1700 nm. The setup was sensitive enough to perform the measurement of the QY down to 0.002%.

The investigation of the UCNPs with fluoride and oxide matrixes showed that the host material based on fluorides (NaYF4) are the most promising environment for the relatively efficient upconversion due to its low phonon energy of ~350 cm^{-1}. However, the special attention should be paid to the material homogeneity, and the quenching effects at the nanoparticle-shell border and due to OH species. The nanoparticles with PVP cover and high content of hydroxyl groups exhibited very weak upconversion signal despite the low phonon energy (300 cm^{-1}). The nanoparticles based on oxide matrix (Y_2O_3) with higher phonon energy (~550 cm^{-1}) demonstrated a slightly lower upconversion efficiency comparing to $NaYF_4$-based host matrix, what is quite predictable result. It is worth to mention that the nanoparticles did not indicate the down-conversion emission, which could give the expectation that the energy transfer process between activator and sensitizer is favourable for upconverison effect, and the visible emission is quenched in the surrounding environment.

The experiments with the phosphate glasses confirmed the strong disadvantage of the high phonon energy matrix (~1200 cm^{-1}) for the upconversion luminescence material. The upconversion emission in the phosphate glasses doped by Er ions was extremely weak,

what did not allow to quantify the QY value. The UCNPs-doped glasses demonstrated better performance in this means. However, the synthesis of such glasses requires special attention to the heat temperature to avoid corrosion of the nanoparticles, which negatively affect the upconversion efficiency. From another side, the addition of metallic nanoparticles such as silver increases the efficiency of the visible emission almost up to the bare nanoparticles value. The question regarding the influence of the outer environment remains open. The high phonon energy material might result in the surface quenching of the luminescence at the nanoparticles-glass border.

The low phonon energy environment, highly homogenous and "water-free" would be an ideal host matrix for the upconversion luminescence material. This was confirmed by the experiments with the tellurite glasses doped by Er/Yb,Er. However, even in this ideal environment with the minimum number of the sources for luminescence quenching, the special attention should be paid to the dopants and its concentration. More specifically, the energy transfer process should be favourable for the upconversion emission only avoiding any down-conversion emission. For this, better results were demonstrated for the classical two ions system, namely activator (Yb^{3+}) and sensitizer (Er^{3+}).

The summary of the QY measurements for the all investigated samples is presented in Table 6.

Sample	**Doping**	**Matrix**	**UC, %**	**DC,%**
		UCNPs		
UCNPs 1.	Er^{3+},Yb^{3+}	$NaYF_4$, (p.e.350 cm-1)	0.6	No
UCNPs 2.	Er^{3+},Yb^{3+}	Y_2O_3:Yb,Er, (p.e 550 cm-1)	0.46	No
UCNPs 3.	Er^{3+}	LaF_3, (p.e 400 cm-1)	-	-
		Phosphate Glass		
Glass P.1	$0.25Er_2O_3$	$75NaPO_3$-$25CaF_2$	-	58.18
Glass P.2	$0.25Er_2O_3$	75NaPO3-$25CaF_2$	-	75.3
Glass P.3	5wt% $NaYF_4$:Er^{3+},Yb^3	$90NaPO_3$-10NaF	0.002	15.3

Glass P.4	5wt% $NaYF_4:Er^{3+},Yb^3$	$83.25NaPO_3$– 9.25NaF–5ZnO- $2.5Ag_2O$	0.43	21.77
Tellurite Glass				
Glass T.1.	Er_2O_3 - 4%	TeO_2-WO_3-La_2O_3-Bi_2O_3 (OH- 0.018 cm^{-1})	0.064	61
Glass T.2.	Er_2O_3 - 1.34%	TeO_2-WO_3-La_2O_3-Bi_2O_3 (OH- 0.005 cm^{-1})	1.1	120.4
Glass T.3.	Er_2O_3 - 0.42%	TeO_2-WO_3-La_2O_3-Bi_2O_3 (OH- 0.006 cm^{-1})	0.93	154
Glass T.4.	Er_2O_3-0,1% Yb_2O_3-0,1%	TeO_2–ZnO–La_2O_3–Na_2O (OH- 0.028 cm^{-1})	0.38	42.8
Glass T.5.	Er_2O_3-0,1%, Yb_2O_3-0,45%	TeO_2–ZnO–La_2O_3–Na_2O (OH- 0.021 cm^{-1})	3.3	52.6

Table 6. The summary of the QY measurements for the investigated luminescence samples.

REFERENCES

[1] Jun, Yong Woong et al. “Addressing the autofluorescence issue in deep tissue imaging by two-photon microscopy: the significance of far-red emitting dyes.” Chemical science vol. 8,11: 7696-7704, 2017.

[2] Nonlinear Frequency Conversion, https://www.rp-photonics.com/nonlinear_frequency_conversion.html [Retrieved 11.03.2019]

[3] Ahrens B. “Down- and up-conversion in fluorozirconate-based glasses and glass ceramics for photovoltaic application”, Paderborn University, 120 p. 2009

[4] Sedlmeier, Andreas & Gorris, Hans H. “Surface modification and characterization of photon-upconverting nanoparticles for bioanalytical applications.” Chemical Society reviews 44, 1526-1560, 2014.

[5] J. F. Suyer, A. Aebischer, D. Biner, P. Gerner, J. Grimm, S. Heer, K. W. Krämer, C. Reinhard, and H. U. Güdel, “Novel materials doped with trivalent lanthanides and transition metal ions showing near-infrared to visible photon upconversion,” Opt. Mater. 27(6), 1111–1130 . 2005.

[6] Bloembergen, N. Solid state infrared quantum counters. Phys. Rev. Lett. 2, 84–85 (1959).

[7] Zhou, B., Shi, B., Jin, D. & Liu, X. “Controlling up-conversion nanocrystals for emerging applications.” Nature nanotechnology 10, 924–936, 2015.

[8] F. Zhang, Photon Upconversion Nanomaterials. Springer, 2015.

[9] Zhang, Wenyan & Yang, Songlin & Li, Jian & Gao, Wei & Deng, Yibing & Dong, Wenping & Zhao, Chengjian & Lu, Gongxuan. “ Visible-to-ultraviolet Upconvertion:

Energy transfer, material matrix, and synthesis strategies.” Applied Catalysis B: Environmental. 206. 2017

[10] Joubert M.-F. ‘Photon avalanche upconversion in rare earth laser materials.” Optical Materials – Vol. 11 – № 2–3 –p.181–203. 1999.

[11] Liu, Ru-Shi. “Phosphors, Up Conversion Nano Particles, Quantum Dots and Their Applications.” 2016.

[12] Dong, Hao & Sun, Ling-Dong & Yan, Chun-Hua. “Energy transfer in lanthanide upconversion studies for extended optical applications.” Chem. Soc. Rev. 2014 .

[13] Yasaka, Patarawagee & Kaewkhao, Jakrapong. “Luminescence from lanthanides-doped glasses and applications: A review.” 4-15. 2015.

[14] Zhou, Jing & Liu, Qian & Feng, Wei & Sun, Yun & Li, Fuyou. “Upconversion Luminescent Materials: Advances and Applications. Chemical reviews”. 2014.

[15] Kuznetsova J.O. “Transfer of electronic exitations in up-conversion nanoparticles containing rare-earth ions.” 2013.

[16] Volkova, E.K. & Yanina, Irina & Popov, Alexey & Bykov, Alexander & Gurkov, Anton & Borvinskaya, Ekaterina & Timofeyev, Maxim & Meglinski, Igor. “Ecophotonics: Assessment of temperature gradient in aquatic organisms using up-conversion luminescent particles. Quantum Electronics.” 47. 153-157. 2017.

[17] C. R. Ronda, Luminescence: From Theory to Applications. Weinheim, Germany: Wiley-VCH Verlag GmbH & Co. KGaA, 2007.

[18] F. Wang, R. Deng, J. Wang, Q. Wang, Y. Han, H. Zhu, X. Chen, X. Liu, “Tuning upconversion through energy migration in core–shell nanoparticles.” Nat Mater 10, 968–973. 2011

[19] C. Strohhöfer , A. Polman. “Absorption and emission spectroscopy in Er^{3+}–Yb^{3+} doped aluminum oxide waveguides.” Optical Materials. 21. P. 705-712. 2003.

[20] Dong H, Sun L-D, Yan C-H. “Energy transfer in lanthanide upconversion studies for extended optical applications.” Chem. Soc. Rev.2015.

[21] Haase, M. and Schäfer, H., “Upconverting Nanoparticles.” Angew. Chem. Int. Ed., 50: 5808-5829. 2011.

[22] Klinkov V.A., Semencha A.V., Tsimerman E.A.” Advanced Materials for Fiber Communication Systems.”. Lecture Notes in Computer Science, vol 10531. Springer, Cham. 2017.

[23] Marcin Kochanowicz, Wojciech Mazerski, Jacek Zmojda, and Dominik Dorosz "Upconversion luminescence in tellurite optical fiber codoped with Yb^{3+}/Ho^{3+} ions", Proc. SPIE 8698, Optical Fibers and Their Applications 2012, 11 January 2013

[24] Boetti, Nadia & Lousteau, Joris & Negro, Davide & Mura, Emanuele & Scarpignato, Gerardo & Abrate, S & Milanese, Daniel.. “Multiple visible emissions by means of up-conversion process in a microstructured tellurite glass optical fiber.” Optics express. 20. 2012.

[25] Wang, Xindong & Valiev, Rashid & Ohulchanskyy, Tymish & Agren, Hans & Yang, Chunhui & Chen, Guanying. “Dye-sensitized lanthanide-doped upconversion nanoparticles.” Chemical Society Reviews. 2017.

[26] Jin, J. and Wong, W. “Lanthanides: Upconversion Nanoparticles for Bioimaging Applications.” In Encyclopedia of Inorganic and Bioinorganic Chemistry, R. A. Scott (Ed.). 2012.

[27] Sedlmeier A, Gorris H.H “Surface modification and characterization of photon-upconverting nanoparticles for bioanalytical applications.” Chem Soc Rev 44:1526–1560. 2015

[28] Li, X., Zhang, F., & Zhao, D. " Lab on upconversion nanoparticles: optical properties and applications engineering via designed nanostructure." Chemical Society Reviews, 44(6), 1346–1378. 2015.

[29] Christian Würth, Markus Grabolle, Jutta Pauli, Monika Spieles, and Ute Resch-Genger. "Comparison of Methods and Achievable Uncertainties for the Relative and Absolute Measurement of Photoluminescence Quantum Yields" Analytical Chemistry. 83 (9), 3431-3439. 2011.

[30] UPB-150-ART Universal integrating sphere for transmission and reflectance applications, https://www.gigahertz-optik.de/en-us/product/UPB-150-ART [Retrieved 15.02.2019]

[31] Acridine Orange, http://www.photochemcad.com/compound-detail.php?name=Acridine%20Orange [Retrieved 26.02.2019]

[32] ZnCdSeS QDs, https://www.mesolight.com/cdsexznsxqds.html [Retrieved 19.02.2019]

[33] Kale, Vishal. "Blue and Uv-Emitting Upconversion Nanoparticles: Synthesis and (Bio) Analytical Applications." 2015.

[34] Ojha N., Tuomisto M., Lastusaari M., Petit L., "Upconversion from fluorophosphate glasses prepared with NaYF4:Er3+,Yb3+nanocrystals." In: RSC Advances. Vol. 8, No. 34. pp. 19226-19236. 2018.

[35] Dousti, M. R., Sahar, M. R., Ghoshal, S. K., Amjad, R. J., & Arifin, R. Up-conversion enhancement in Er3+-Ag co-doped zinc tellurite glass: Effect of heat treatment. Journal of Non-Crystalline Solids, 358(22), 2939–2942. 2012.

[36] V. V. Dorofeev, A. N. Moiseev, M. F. Churbanov, V. G. Plotnichenko, A. F. Kosolapov, and E. M. Dianov, "Characterization of high-purity tellurite glasses for fiber optics," in Advanced Photonics, OSA Technical Digest (CD). 2011.

[37] Churbanov́, M.F. & Moiseev, A.N. & Chilyasov, A.V. & Dorofeev, Vitaly & Kraev, I.A. & Ltpatova, M.M. & Kotereva, Tatiana & Dianov, Evgeny & Plotnichenko, V.G. & Kryukova, E.B. “Production of high-purity TeO2-ZnO and TeO2-WO 3 glasses with the reduced content of OH-groups.” Journal of Optoelectronics and Advanced Materials. 9. 3229-3234. 2007.